European Journal of Medicinal Chemistry 290 (2025) 117552

Contents lists available at ScienceDirect

European Journal of Medicinal Chemistry

journal homepage: www.elsevier.com/locate/ejmech

Research paper

O-derivatization of natural tropolone and β-thujaplicin leading to effective inhibitors of human carbonic anhydrases IX and XII

Francesco Melfi [a,1], Ilaria D'Agostino [b,1], Simone Carradori [a,*], Fabrizio Carta [c,**], Andrea Angeli [c], Giosuè Costa [d,e], Gioele Renzi [c], Ana Čikoš [f], Daniela Vullo [c], Josip Rešetar [a], Marta Ferraroni [g], Chiara Baroni [g], Francesca Mancuso [h], Rosaria Gitto [h], Francesca Alessandra Ambrosio [d], Emanuela Marchese [d], Roberta Torcasio [i,j], Nicola Amodio [i], Clemente Capasso [k], Stefano Alcaro [d,e], Claudiu T. Supuran [c]

[a] *Department of Pharmacy, "G. d'Annunzio" University of Chieti-Pescara, 66100, Chieti, Italy*
[b] *Department of Pharmacy, University of Pisa, 56126, Pisa, Italy*
[c] *Neurofarba Department, University of Florence, Sesto Fiorentino, 50019, Florence, Italy*
[d] *Dipartimento di Scienze della Salute, Università "Magna Græcia" di Catanzaro, Campus "S. Venuta", 88100, Catanzaro, Italy*
[e] *Net4Science Academic Spin-Off, Università "Magna Græcia" di Catanzaro, Campus "S. Venuta", 88100, Catanzaro, Italy*
[f] *NMR Centre, Ruđer Bošković Institute, Bijenička cesta 54, 10000, Zagreb, Croatia*
[g] *'Ugo Schiff' Chemistry Department, University of Florence, Via della Lastruccia 3, 50019 Sesto Fiorentino, Florence, Italy*
[h] *Department of Chemical, Biological, Pharmaceutical, and Environmental Sciences, University of Messina, Viale F. D'Alcontres 13, 98166, Messina, Italy*
[i] *Department of Experimental and Clinical Medicine, University "Magna Græcia" of Catanzaro, Campus "S. Venuta", 88100, Catanzaro, Italy*
[j] *Department of Biology, Ecology and Earth Sciences (Di.B.E.S.T.), University of Calabria, 87036, Rende, Italy*
[k] *Department of Biology, Agriculture and Food Sciences, Institute of Biosciences and Bioresources, CNR, Napoli, Italy*

ARTICLE INFO

Keywords:
Tropolone
Thujaplicin
Carbonic anhydrase
Cancer
Regioisomer
Multiple myeloma

ABSTRACT

Herein we report the chemical derivatization of the naturally occurring Tropolone (**TRP**) and its related compound β-Thujaplicin (β-**TJP**) as well as their *in vitro* assessment for inhibition of the physio/pathologically relevant hCAs isoforms I, II, VA; VII, IX and XII to obtain a first set of inhibition data useful for driving selected derivatives towards appropriate biomedical exploitation. The selected compound **17β** was characterized for its chemical stability and assessed for its antiproliferative activity on a multiple myeloma model and showed potent pro-apoptotic features jointly with a safe toxicity profile on healthy cells. The binding mode of β-**TJP** within the hCA II was assessed by means of X-ray crystallography of the hCA II/β-**TJP** complex and showed almost complete superposition with the hCA II/**TRP** adduct reported in the literature. The data produced were used to elaborate a binding prediction model of such compounds on the hCAs VA, IX, and XII which are directly connected to important diseases. Overall, the achievements reported in this work are in the sustainment of the exploitation of naturally occurring troponoloid-based structures for biomedical purposes and thus contribute to the field in extending the variety of available chemical features.

1. Introduction

Tropolone (**TRL**, Fig. 1), also known as hydroxytropone, is a seven-membered aromatic compound endowed with a cyclic ketone function and a vicinal enolic hydroxyl group. The latter seems to correspond to a combination of enol and phenol properties. Besides the peculiar acidity, the presence of the two moieties makes **TRP** be regarded as a vinylog of carboxylic acids, and in some cases, an effective bioisostere of benzoic acid [1]. In this context, it is recognized to establish a strong intramolecular and intermolecular association due to an H-bond and to be able to chelate metals through the two oxygen atoms of the molecule [2,3] (Fig. 1).

* Corresponding author.
** Corresponding author.
E-mail addresses: simone.carradori@unich.it (S. Carradori), fabrizio.carta@unifi.it (F. Carta).
[1] The authors contributed equally to this work.

https://doi.org/10.1016/j.ejmech.2025.117552
Received 18 February 2025; Received in revised form 20 March 2025; Accepted 21 March 2025
Available online 27 March 2025

The exceptional structure of **TRP** came from natural sources and in particular it is produced by bacteria, fungi, and yeast, and was identified for the first time as a virulence factor of a plant pathogen [4]. In addition, different cyclization synthetic approaches have been reported to obtain the **TRP** nucleus in the laboratory [5–7]. However, it is often found as part of more complex natural compounds, such as colchicine [8], and about 200 molecules have been identified as natural **TRP**s [9]. **TRP** has been widely investigated for its antioxidant properties as well as its antibacterial, antiparasitic [10], and in general, antimicrobial [11] properties. On the basis of its polypharmacology, **TRP** is hypothesized to act by perturbing microbial membranes [12] and metabolism, especially due to its ionophoric, thereby metal chelating, action [13,14].

However, among tropolonoids, thujaplicins (**TJP**s, Fig. 1) attracted the interest of the scientific community. This class of compounds bears an isopropyl group in different positions of the **TRP** core, such as C2, C3, and C4, resulting in α-, β-, and γ-**TJP** (Fig. 1), respectively, with the Greek alphabet referring to the functionalization position with respect to the OH moiety (Scheme 1). Naturally occurring from certain coniferous trees, mainly the Cupressaceae family, *e.g.*, *Thuja* species, which has conferred the name to the derivatives. β-**TJP**, also known as Hinokitiol, found large applications in cosmetics, food, oral care, and beauty products due to its antioxidant [15], antimicrobial [16], anticancer [17], antidiabetic [18], and other activities. Multiple pharmacological potentialities of tropolonoids are associated with the chelating properties of the α-enolic ketone moiety, resulting in a bidentate ligand coordinating the metal ions [19], able to act as ionophores [20], or siderophores [21], thereby, affecting the homeostasis of metals in the cell cytoplasm or depleting the levels of metal cofactors and as modulators of enzymes function by impairing their folding or their catalytic activity.

Moreover, several X-ray structures of **TRP**-metalloenzyme complex have been deposited in the Protein Data Bank database (PDB, https://www.rcsb.org), *i.e.*, those of human tyrosinase-related protein 1 [22] and human Carbonic Anhydrase (hCA) II isoenzymes [3](discussed later), proving the zinc-binding properties of the nucleus. Also, several contrast agents with a tropolonoid-based structure have been reported [23].

Notably, a previous study by Cohen and coworkers reported the inhibitory activity of **TRP** and **TJP** towards hCA II, a human (h) isoenzyme of the superfamily of CAs (EC: 4.2.1.1), metalloenzymes catalyzing the hydration of carbon dioxide into bicarbonate ion and proton. Along with a large series of compounds, the two natural troponoloids were investigated on their ability to chelate the zinc ion, the cofactor of the enzyme. The study revealed low inhibition percentages (Inhib. % = 16–17 %) for both compounds when tested at 500 μM on the wild-type isoenzyme by means of the 4-nitrophenylacetate esterase assay. Remarkably, kinetic studies on two hCA II variants, *i.e.,* H94C and H94D, revealed a drop in the inhibitory activity (Inhib. % = 0%) and an increase in potency (Inhib. % = 47–49%), respectively, proving a specific interaction network in the active site of the enzyme [24]. Some years later, the same group reported **TRP** and its isostere thiotropolone (**TTRP**) (illustrated in Fig. 1 in one of the tautomeric forms) to inhibit the wild-type hCA II with inhibition constant (K_I) values of 1350 and 96 μM, respectively, proving the importance of the sulfur atom in the metal binding ability of such compounds. Again, in this study, the enzymatic assays on a different variant, hCA II L198G, containing a glycine residue in place of a leucine, led to an increase in the potency of both compounds (K_Is = 245 and 61 μM, respectively). X-ray crystallization studies confirmed the zinc-binding ability of **TRP** [3]. One year earlier, Costa et al. performed a structure-based virtual screening on a library of essential oils aimed at discovering new inhibiting chemotypes of the mitochondrial hCA VA, an isoform involved in lipogenesis and associated with obesity. During this study, β-**TJP** emerged and deeper *in silico* studies, *i.e.,* molecular dynamic simulations, confirmed the role of the tropolonoid zinc binding group in the interaction with the enzyme and enzymatic assays assessed a micromolar inhibition of hCAs I, II, and VA, with K_I values of 4.98, 90.60, and 7.50 μM, respectively [25]. Altogether, the potentialities of tropolonoids in inhibiting CAs and the multifaceted physiopathological role of these enzymes led us to investigate **TRP** and **TJP** core by generating a library of *O*-functionalized derivatives as putative inhibitors of representative α-CAs belonging to humans (main text) or other microorganisms (Table S1 in the Supplementary Material file).

2. Results and discussion

2.1. Synthesis of tropolonoid derivatives

Aimed at exploring the chelating properties of **TRP** and β-**TJP**, different *O*-functionalized derivatives were developed and, in particular, ethers and esters were prepared by reacting the tropolonoid nuclei with the suitable chemical, mainly halide, in a basic environment (Scheme 1).

For these reactions, the presence of a base, being inorganic as K_2CO_3 or organic as *N,N,N*-triethylamine (TEA) and *N,N*-dimethylaminopyridine (DMAP), all characterized by a pK_a of approximately 10, is necessary to allow the complete deprotonation of the enolic group of the tropolonoid making it to act as a nucleophile. However, instead of **TRP**, the treatment of β-**TJP** with such bases leads to the generation of two resonance forms, namely the β- and the δ-**TJP** enolates, and the following nucleophilic attack generates the corresponding β- and the

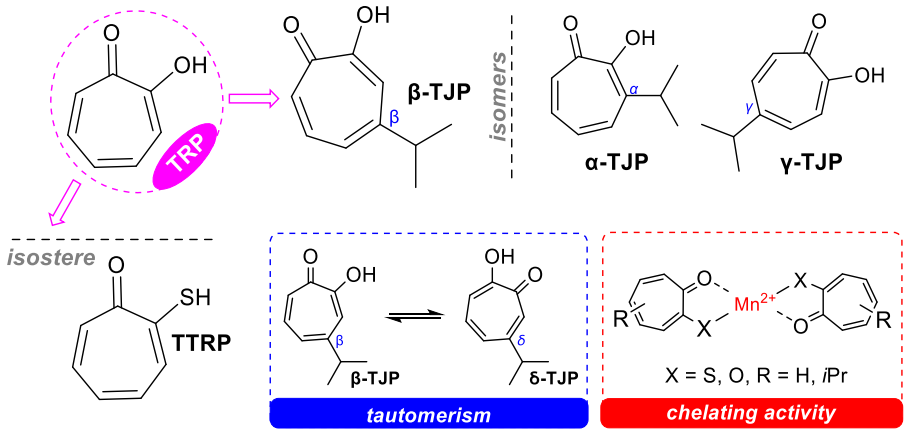

Fig. 1. Chemical structure of natural tropolone (**TRP**) and β-thujaplicin (β-**TJP**, or Hinokitiol) with the latter isomers α-thujaplicin (α-**TJP**) and γ-thujaplicin (γ-**TJP**) along with the synthetic derivative thiotropolone (**TTRP**). A representative example of tautomerism (β-δ **TJP**) and the mechanism of chelation are illustrated in the blue and red boxes, respectively. (For interpretation of the references to colour in this figure legend, the reader is referred to the Web version of this article.)

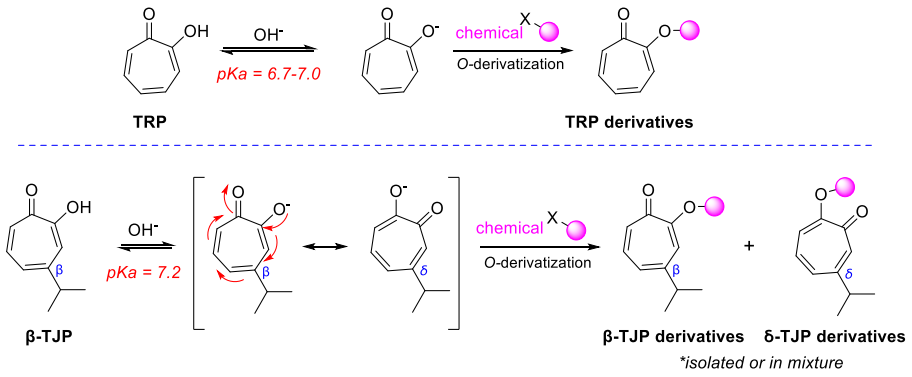

Scheme 1. General reaction scheme involving *O*-derivatization on **TRP** or β-**TJP** in basic environment, generating **TRP** derivatives and β- and δ-**TJP** derivatives. pK_a values for **TRP** and β-**TJP** are reported [5].

δ-**TJP** adducts (Scheme 1), as already reported [26–28]. However, the isolation and identification of the two **TJP** regioisomers are not a trivial job and require in-depth investigations, often based on a combination of NMR experiments. In detail, a large library of **TRP** and **TJP** derivatives was synthesized through different *O*-derivatization reactions, as depicted in Scheme 2.

First, *O*-alkylation (*i*, Scheme 2) was performed via nucleophilic substitution by using the suitable halogen derivative (R^1X) in a basic environment for potassium carbonate, furnishing **TRP** derivatives **1–3**, **7–13**. Interestingly, when we employed β-**TJP** as the starting material, in most cases the two β- and δ-regioisomers were generated. The isolation of both the pure regioisomers was successful only when the *O*-benzyl function was functionalized in the *ortho* position, *e.g.,* the 2-nitrobenzyloxy **TJP**s **11β** and **11δ** and the 2-trifluoromethylbenzyloxy derivatives **12β** and **12δ**. However, when the nitro group was moved to the *para* or *meta* position, the two **TJP** regioisomers were not isolated and a 50:50 mixture was obtained (**9β+δ** and **10β+δ**, respectively). Similar results were obtained for *O*-propargylated (**1β+δ**), *O*-chloropropyl (**2β+δ**), 4-cyano benzyloxy (**8β+δ**), and 2-(5-phenyl-1,3,4-oxadiazolyl)methoxy (**14β+δ**) **TJP**s with β:δ ratios close to 50:50 (with the exception of **1β+δ** with 55:45 ratio). Otherwise, in some cases, we isolated just one pure regioisomer and, in particular, 4-bromo benzyloxy **TJP 7δ** and the 1-naphthylmethoxy **TJP 13δ** in a reaction yield (= 52% in both cases) comparable to the others, thereby, we could assume they were the only regioisomer produced from the reaction.

The *O*-alkylation with ethyl bromoacetate led to derivatives **5** and **5β+δ**, which were then hydrolyzed by lithium hydroxide to free carboxylic acids **6** and **6β+δ** (*ii*, Scheme 2). Also, for these **TJP**s, the regioisomer mixture was not solved. Interestingly, we synthesized a **TJP** dimeric compound (**4δ**) by reacting 1,5-dibromopentane with an excess

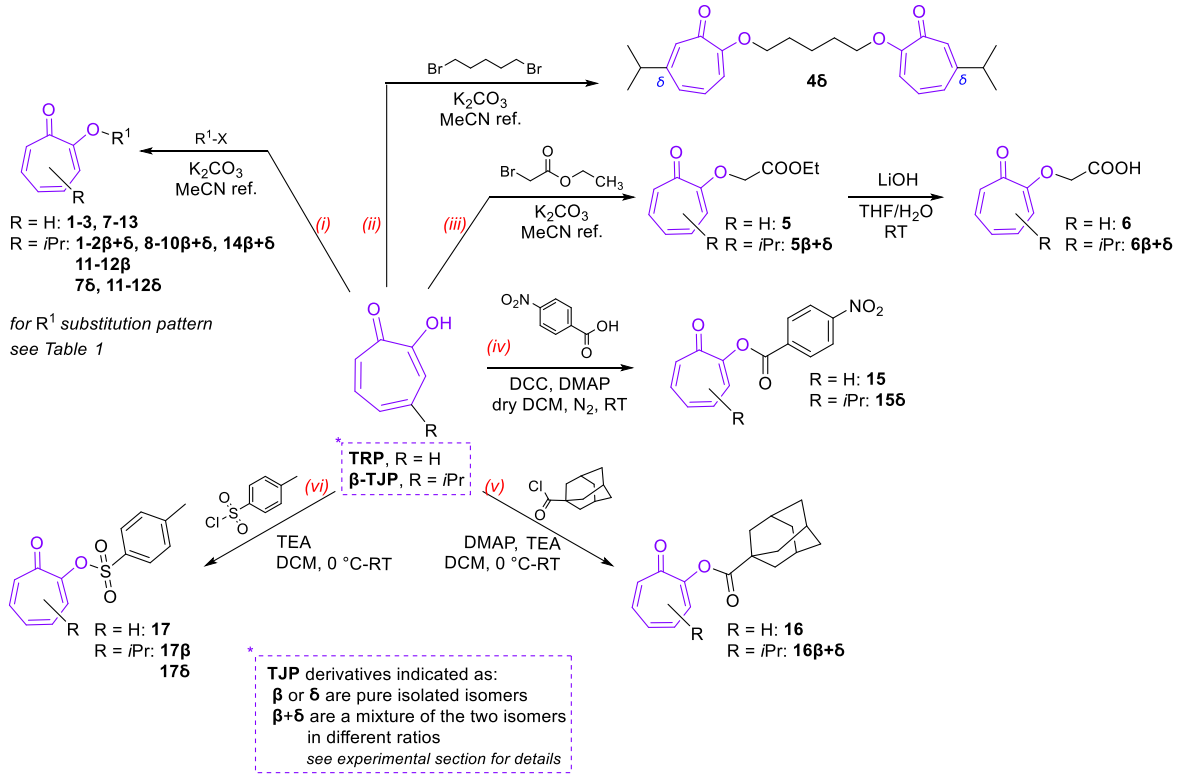

Scheme 2. Synthetic pathways for the preparation of **TRP** and **TJP** derivatives **1–17**. **TRP** (R=H) and **TJP** (R = *i*Pr) derivatives. The numbering code with Greek letters **β** or **δ** indicates the position of the isopropyl moiety on the **TJP** scaffold with respect to the hydroxyl group, as conventional (see Fig. 1). Compounds indicated as **β+δ** are a mixture of the two isomers in different ratios (see *Experimental Section* for details). The R^1 substitution pattern is reported in Table 1.

of β-**TJP** (*iii*, Scheme 2). The ^{1}H and ^{13}C NMR analysis for this compound highlighted the presence of δ-**TJP** scaffolds. Also, we prepared 4-nitrobenzoyl and adamantanoyl derivatives by reacting the tropolonoids with the suitable carboxylic acid or acyl chloride and, apart from the **TRP** derivatives **15** and **16**, the δ-**TJP** regioisomer **15δ** was isolated as the only product whereas the adamantanoyl **TJP** derivative was obtained as a regioisomeric mixture (**16β+δ**) (*iv*, Scheme 2). Peculiarly, the latter was the only case of a product with a β:δ ratio of 85:15 with a large preference for β-**TJP** regioisomer, resulting in being the major isomer.

In the end, tosylation of the OH moiety of **TRP** and β-**TJP** was performed by using tosyl chloride, and the corresponding tosylates **17**, **17β**, and **17δ** were afforded (Scheme 2). In this case, the products were already characterized and structures elucidated, although obtained through different reaction conditions, *e.g.,* by using pyridine as a base [28].

As already mentioned, we successfully isolated the two regioisomers obtained in the synthetic pathway. However, in some cases, although we did attempt to separate the regioisomers via direct phase, silica gel-based column chromatography, and employing various eluent conditions, the regioisomers often co-eluted, making the full separation not feasible. This could be due to their small structure and high structural similarity. As a result, we tested the mixture of regioisomers and relied on in-depth NMR techniques to determine their ratio for the reaction yield characterization and the following biological evaluation.

2.2. Insight into the chemical structure of TJP regioisomers mixtures 10β+δ and 8β+δ and pure products 11β and 11δ via NMR experiments

In order to elucidate the chemical structure of the **TJP** regioisomers, combined bidimensional NMR experiments were performed. In particular, Heteronuclear Single Quantum Correlation (HSQC), Heteronuclear Multiple Bond Correlation (HMBC) NMR and Nuclear Overhauser Effect Spectroscopy (NOESY) techniques were employed on the two β and δ regioisomers of two different **TJP**s (**10β+δ**) and **8β+δ**. The former experiments are generally used to determine the correlation of ^{1}H and ^{13}C nuclei single bonds (HSQC) and the nuclei separated by two, three, or more bonds. NOESY, instead, provides information on through-space nuclei interactions (see NMR spectra in the Supplementary Material file, Figs. S25–S28 and S37–S40). Interestingly, the analysis of HMBC NMR spectra for the investigated compounds **10β+δ** and **8β+δ** revealed two sets of resonance lines corresponding to two regioisomers in each sample (Fig. 2).

The main evidence for the unambiguous structural assignment of these compounds lies in the carbon chemical shift of atoms numbered 3. All four compounds analyzed show a ^{1}H–^{13}C HMBC interaction between the methyl doublets 9,10-CH_3 and 8-C, which in turn show interaction with 3-H. Based on the knowledge of the proton chemical shift of 3-H, its associated carbon can be easily identified from the ^{1}H–^{13}C HSQC spectrum. In the β isomers (marked in blue in Fig. 1), the 3-C chemical shifts are 118.0 ppm and 117.6 ppm for **10β+δ** and **8β+δ**, respectively. Both δ-**TJP** isomers (marked in red in Fig. 2) exhibit a carbon chemical shift of 3-C at 135.0 ppm. Additional confirmation for the elucidated structures was found in the NOESY spectra, in which both β-**TJP** isomers show a strong NOE interaction between 11-CH_2 and 3-H, while their δ-**TJP** counterparts exhibit the cross-peak between 11-CH_2 and 7-H. NMR analysis for pure isolated regioisomers **11β** and **11δ** was similar. In the β-**TJP** isomer (**11β**), the carbon chemical shift of 3-C is 117.0 ppm, while in the δ-**TJP** isomer (**11δ**) 3-C is found at 134.9 ppm. Analysis of NOE contacts (Fig. 3) confirmed the assignment.

Thanks to this analysis, the structure elucidation of the pure **TJP** regioisomers and the assessment of the β:δ ratio in the mixture was performed and helped the structure-activity relationships (SARs) and *in silico* further studies.

2.3. Inhibitory activity against α-carbonic anhydrases and SARs considerations

TRP compounds along with **TJP** derivatives as pure regioisomers or their mixture were tested against a panel of α-CAs endowed with specific physio-pathological roles, belonging to humans (hCAs I, II, VA, VII, IX, and XII) (Table 1), bacteria (VchCAα from *Vibrio cholerae* [29] and HpCAα from *Helicobacter pylori* [30]), protozoa (TcCAα from *Tripanosoma cruzi* [31]), and parasites (SmCAα *from Schistosoma mansoni* [32]) to further assess potency and isoform selectivity (Table S1).

All the synthesized compounds turned out to be less potent than the reference compound, acetazolamide (**AAZ**). The large dataset (Table 1) allowed the establishment of preliminary SARs which are herein reported based on the isoform.

- As regards the parent compounds, **TRP** did not show any activity on hCA I whereas β-**TJP** exhibited a low micromolar inhibitory activity (K_I = 4.98 μM). The majority of **TRP** and **TJP** derivatives were found almost all inactive towards this isoform. The most potent compound,

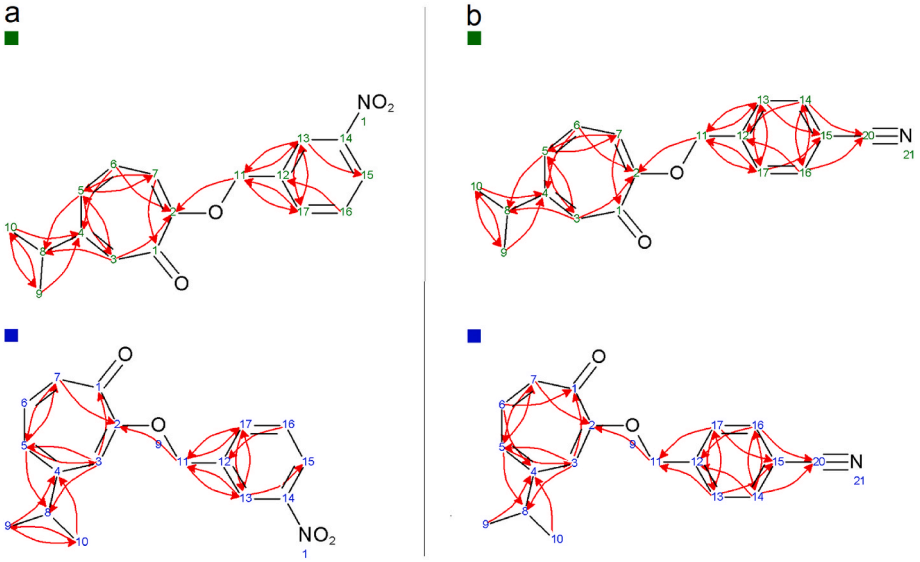

Fig. 2. Structure, numbering, and key ^{1}H–^{13}C HMBC interactions marked with red arrows for β-**TJP** (blue) and δ-**TJP** (green) for compounds (a) **10β+δ** and (b) **8β+δ**. (For interpretation of the references to colour in this figure legend, the reader is referred to the Web version of this article.)

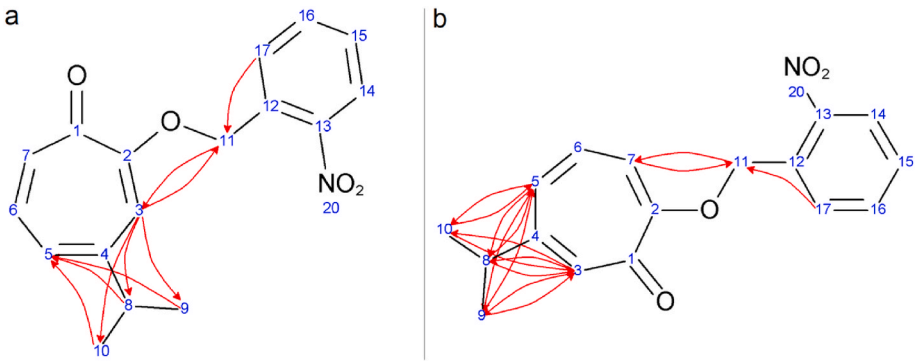

Fig. 3. Structure, numbering, and key $^{1}H–^{1}H$ NOESY interactions marked with red arrows for β-**TJP** and δ-**TJP** regioisomers of compounds (a) **11β** and (b) **11δ**. (For interpretation of the references to colour in this figure legend, the reader is referred to the Web version of this article.)

the *O*-propargylated **TRP** derivative **1** showed a K_I of 0.05 μM, while the corresponding mixture of β- and δ-**TJP**, namely **1β+δ**, resulted in being active as well, but less potent ($K_I = 0.66$ μM). Moreover, 4-cyanobenzyloxy (**8**), 4-nitrobenzyloxy (**9**), and 2-nitrobenzyloxy (**11**) **TRP** derivatives exhibited moderate results with K_I of 8.31, 6.22, and 8.01 μM, respectively, suggesting that nitro group led to inhibitory activity on hCA I only in *para* or *ortho* positions, whereas when in *meta*, as compound **10**, this electron-withdrawing function led to a decrease in potency ($K_I > 100$ μM).

- **TRP** and β-**TJP** were found inefficacious in inhibiting the physiologically relevant hCA II, whereas some derivatives showed a micromolar inhibition, thus confirming the *O*-derivatization to determine a gain in potency. In detail, the **TJP** isomers mixture of 3-chloropropyl (**2β+δ**) and 2-phenyl-oxadiazolyloxy (**14β+δ**) derivatives exhibited K_I values of 2.95 and 2.80 μM against hCA II, respectively, representing the most active derivatives of the series. Other promising compounds are the **TRP**-based compound with the acetyl moiety (**6**), 1-naphthylmethylene-oxy-**TRP** (**13**), and **13δ** with K_I values between 3.02 and 3.96 μM, and to a lesser extent, compound **4δ**, with alkyl linker between the two δ-**TJP**s, 4-bromobenzyloxy δ-**TJP** (**7δ**), 4-nitrobenzoate δ-**TJP** (**15δ**), and *p*-toluenesulfonate **δ-TJP** (**16δ**) with K_I values between 6.39 and 8.72 μM.
- Most of the synthesized compounds resulted in being inefficacious inhibiting hCA VA, with the best-in-class compound being the tosylate **17δ**, with a K_I value of 4.45 μM. It is interesting to note that the β-**TJP** analogue (**17β**, $K_I = 39.0$ μM) exhibited weaker inhibitory activity, whereas *p*-toluenesulfonate tropolone **17** was completely inactive on hCA VA ($K_I > 100$ μM), highlighting the importance of the presence of isopropyl group nearby ketone moiety instead of *O*-sulfonyl one, while compounds **2**, **2β+δ**, **6**, **7δ**, **11β**, and **12** exhibited K_i values between 6.63 and 9.56 μM. In detail, the **TRP** scaffold was favored than **TJP** core for compounds **2** ($K_I = 8.75$ μM) and **2β+δ** ($K_I = 9.56$ μM), while the elongation of the alkyloxy tail with two methylene moieties, and the substitution of chlorine with the bigger and more electron-withdrawing bromine, as in compound **3**, led to a dramatically decrease of activity of tropolone scaffold ($K_I = 84.16$ μM). Tropolone scaffold was recommended for acetyl derivatives (**6**, $K_I = 8.11$ μM), where the presence of isopropyl group led to an inefficacious compound (**6β+δ**, $K_I > 100$ μM). Among the benzyloxy derivatives, **TJP** was favored for 4-bromo- (**7δ**, $K_I = 7.95$ μM), and 2-nitrobenzyloxy (**11β**, $K_I = 8.96$ μM; **11δ**, $K_I = 21.67$ μM) compounds, whereas the substitution of the nitro group with the other electron-withdrawing trifluoromethyl one, in position 2, led to stronger results for tropolone derivative **12**, instead of TJP ones **12β** and **12δ**, with K_I values of 6.63, 83.51, and >100 μM, respectively. Further, independently from **TRP** and **TJP** scaffolds, the nitro group was not tolerated only in positions 4 (**9**, **9β+δ**, $K_I > 100$ μM) and 3 (**10**, **β+δ**, $K_I > 100$ μM). Moreover, β-**TJP** was moderately active in the inhibition of hCA VA, with a K_i of 7.50 μM.
- Both **TRP** and β-**TJP** did not display activity on hCA VII, while some of their derivatives showed a better profile. In particular, 4-bromobenzyloxy δ-**TJP** (**7δ**) exhibited a K_I of 0.96 μM, resulting in being the most potent derivative in this context, while its **TRP** analogue (**7**) resulted to be completely inactive, with K_I value > 100 μM. Among the alkyl derivatives, compounds **2**, **2β+δ**, and **3** exhibited moderate inhibitory activity on hCA VII, with K_I values of 5.20, 2.78, and 1.52 μM, respectively. The absence of isopropyl group of **6** increased more than 14-fold the inhibitory activity (**6**, $K_I = 4.87$ μM; **6β+δ**, $K_I = 71.3$ μM). Conversely, for benzyloxy compounds, **TRP** was not the first choice to reach potent hCA VII inhibitors, except for 2-trifluoromethyl derivative **12**, with K_I of 6.19 μM. Among the nitro derivatives, position 3 led to the most potent compound **10β+δ** ($K_I = 2.78$ μM) than position 4 (**9β+δ**, $K_I = 33.91$ μM) and position 2 (**11β**, $K_I = 5.41$ μM; **11δ**, $K_I = 6.18$ μM). It is interesting to note that the 4-nitrobenzoate, **15δ**, structurally similar to **9β+δ** resulted in being 3.5-fold more active. These data could be explained by the presence of carbonyl moiety, capable of accepting H-bonds, or for the presence of the single δ regioisomer. Nonetheless, δ-regioisomer led to slightly stronger inhibitory activity for *p*-tosylate derivatives (**17β**, $K_I = 9.33$ μM; **17δ**, $K_I = 5.27$ μM). Lastly, the bulkier naphthylmethylene-oxy moiety showed moderate inhibitory activity, where the **TRP** scaffold was more active than δ-**TJP** (**13**, $K_I = 2.82$ μM; **13δ**, $K_I = 3.95$ μM).
- As regards the two tumor-associated isoenzymes IX and XII, β-**TJP** emerged for moderate activity versus hCA IX ($K_I = 23.88$ μM). Several derivatives showed strong activity in the inhibition of hCA IX, with K_I values less than 1 μM. Indeed, the most active compounds against hCA IX are: **3** ($K_i = 0.54$ μM), **7δ** ($K_i = 0.26$ μM), **8β+δ** ($K_i = 0.44$ μM), **11δ** ($K_i = 0.94$ μM), **13δ** ($K_i = 0.53$ μM), **14β+δ** ($K_i = 0.49$ μM), **15δ** ($K_i = 0.37$ μM), **17β** ($K_i = 0.42$ μM), **17δ** ($K_i = 0.40$ μM). Other promising compounds are **1β+δ**, **2β+δ**, **4δ**, **6β+δ**, **10β+δ**, **11β**, **12**, **13** with K_I values between 1.41 and 4.30 μM. The bromo-alkyl **TRP 3** was the most selective compound toward hCA IX over hCA I and II, with a Selectivity Index (SI) > 185 for both hCA I and II (Selectivity Index was calculated as K_I of hCA I or II/K_I of hCA IX or XII). Whereas, the most potent compound, **7δ**, was not a selective hCA IX inhibitor, with a SI of 28.6 over hCA II. The replacement of bromine with another electron-withdrawing group as cyano in position 4 (**8β+δ**) led to a slight decrease of activity on hCA IX as well as an increase of selectivity over hCA II (SI = 159.6). If on the one hand nitro group did not show strong activity in positions 4 (**9** and **9β+δ**) and 3 (**10** and **10β+δ**), on the other hand, this moiety was suitable in position 2, especially for β- and δ-derivatives. Indeed, **11β** showed a K_I of 1.41 μM and the most active and selective **11δ** exhibited a K_I of 0.94 μM. The substitution of the nitro group in position 2 with trifluoromethyl one (**12β** and **12δ**) led to a dramatical decrease in activity, especially for δ-**TJP** scaffold. Further, the

Table 1
Inhibition data of **TRP**, **TJP**, and their derivatives, and reference compound **AAZ** on a panel of human (h) CA isoforms through the stopped-flow CO_2 hydration assay [33].

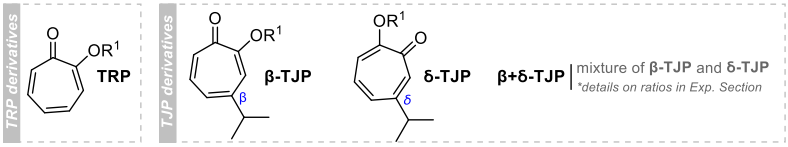

CPD	Core	R^1	K_I (μM)					
			hCA I	hCA II	hCA VA	hCA VII	hCA IX	hCA XII
TRP	TRP	-H	>100	>100	>100	>100	>100	>100
TJP	TJP	-H	4.98[a]	90.6	7.50	>100	23.9	>100
1	TRP		0.05	>100	>100	>100	19.0	7.76
1β+δ	TJP		0.66	76.0	>100	>100	2.29	>100
2	TRP		>100	44.5	8.75	5.20	8.94	6.74
2β+δ	TJP		>100	2.95	9.56	2.78	3.77	7.50
3	TRP	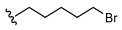	>100	>100	84.2	1.52	0.54	6.21
4δ	TJP	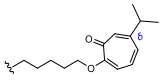	>100	6.36	31.6	7.10	1.33	73.7
6	TRP		>100	3.96	8.11	4.87	25.6	4.24
6β+δ	TJP		>100	>100	>100	71.3	2.53	6.36
7	TRP	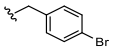	>100	>100	>100	>100	37.7	6.07
7δ	TJP		>100	7.44	7.95	0.96	0.26	4.57
8	TRP	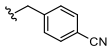	8.31	>100	>100	>100	>100	1.35
8β+δ	TJP		>100	70.2	14.2	9.62	0.44	8.09
9	TRP	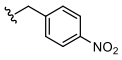	6.22	3.43	>100	>100	13.3	0.99
9β+δ	TJP		>100	>100	>100	33.9	39.5	5.84
10	TRP		>100	>100	>100	>100	34.5	2.64
10β+δ	TJP		>100	>100	>100	2.78	2.73	4.71
11	TRP		8.01	27.6	>100	>100	>100	1.60
11β	TJP		>100	41.4	8.96	5.41	1.41	4.52
11δ	TJP		>100	>100	21.7	6.18	0.94	3.57
12	TRP		>100	>100	6.63	6.19	4.30	3.11
12β	TJP		>100	>100	83.5	>100	47.4	54.6
12δ	TJP		>100	>100	>100	>100	>100	2.08
13	TRP	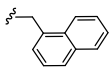	>100	3.70	61.1	2.82	2.28	7.28
13δ	TJP		>100	3.02	89.4	3.95	0.53	5.31
14β+δ	TJP	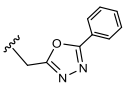	>100	2.80	>100	5.73	0.49	5.03
15	TRP	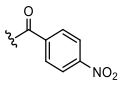	84.4	43.9	>100	>100	>100	1.20
15δ	TJP		>100	8.72	>100	9.60	0.37	5.23
16	TRP		>100	>100	85.6	>100	43.5	2.11
16β+δ	TJP		>100	>100	>100	>100	38.1	3.52
17	TRP		94.2	80.9	>100	>100	>100	>100
17β	TJP		>100	>100	39.0	9.33	0.42	4.37
17δ	TJP		>100	6.97	4.45	5.27	0.40	8.09
AAZ	Reference compound		0.25	0.01	0.06	0.002	0.03	0.01

K_I values are reported as means of three independent experiments. Errors are in the range of ± 5–10 % of the reported values.

presence of naphthylmethylene-oxy (**13**, K_I = 2.28 μM; **13β**, K_I = 0.49 μM) and 2-phenyloxadiazole (**14β+δ**, K_I = 0.49 μM) moieties led to selectivity only over hCA I. It is interesting to note that among the ester compounds, **TJP** scaffold always led to the strongest activity on hCA IX, indeed **15δ** was more than 270-fold stronger than **15**, while **17β** and **17δ** were 238- and 250-fold more active than **17**, respectively. Even though **17β** (SI > 238) was slightly weaker than **17δ**, the latter was less selective over hCA II (SI = 17.4).

- **TRP** and β-**TJP** resulted in being both inactive on hCA XII, nevertheless, their derivatives did not show strong inhibitory activity as for hCA IX, but, it is worth-noting that the strongest compounds are benzyloxy-**TRP** derivatives, like **8** (K_I = 1.35 μM), **9** (K_I = 0.99 μM), **10** (K_I = 2.64 μM), **11** (K_I = 1.60 μM), **15** (K_I = 1.20 μM), and **16** (K_I = 2.11 μM). All these compounds, except for the latter one, bear a nitro group. The adamantanoyl **16** was the most selective towards hCA XII over hCA I and II, with an SI of 47 for both isoforms. It is interesting to note that the introduction of acyl moiety in compound **15** led to a slight decrease (1.21-fold) of inhibitory activity with respect to **9**. **TRP** scaffold seems to be preferable, except for naphthylmethylene-oxy (**13**, K_I = 7.28 μM; **13β+δ**, K_I = 5.31 μM) and *p*-tosylate (**17**, K_I > 100 μM; **17β**, K_I = 4.37 μM; **17δ**, K_I = 8.09 μM) compounds.

In Fig. 4 the general SAR analysis about **TRP**- and **TJP**-derivatives as hCAs IX and XII inhibitors:

The significance of such inhibitory data could be assessed within the context of previously reported hCA inhibitors. In fact, the hCAs inhibitors landscape includes several chemical classes, with most potent chemotypes, such as benzenesulfonamides, are typically endowed with K_I values in the nanomolar or even sub-nanomolar range. However, they often suffer from a lack of isoform selectivity [34,35]. In contrast, coumarins, although being less potent (in the medium-to-high nanomolar range) show a better isoform selectivity, with a typical preference for isoforms other than the physiologically relevant hCAs I and II [36]. Conversely, inorganic ions are reported as high-micromolar or even millimolar inhibitors, with little discrimination among the isoforms [37], whereas phenols and polyphenols generally exhibit micromolar potency on several hCA isozymes [38,39].

In the light of such considerations, the herein-described tropolonoids, despite not exhibiting high inhibitory potency against the tested hCAs, seem to demonstrate a good isoform preference. Unfortunately, potency and selectivity of their inhibition do not follow a clear trend, as the compounds activity and selectivity vary on a case-by-case basis, depending on the structural features of each compound, as highlighted by the performed SAR analysis and summarized in Fig. 4.

2.4. Crystallographic structure of hCA II and β-TJP complex

The investigation of the binding poses of the compounds in the enzyme catalytic pocket started with crystallization studies on β-**TJP**. The crystallographic structure of hCA II complexed with β-**TJP** was obtained by soaking crystals of the enzyme in the inhibitor solution. Analysis of the electron density maps showed a clear density for the studied ligand, confirming its binding to the enzyme. The ligand forms bidentate coordination with the catalytic Zn(II) ion, with Zn–O bond distances of 2.17 and 2.20 Å (Fig. 5A). In the β-**TJP**-hCA II structure, the aromatic ring of the ligand establishes hydrophobic interactions with L198 and V121. Moreover, one of the oxygens on the β-**TJP** ring forms water-bridge hydrogen bonds with the peptide NH and the OH of T199, similar to the well-known interactions formed by the traditional

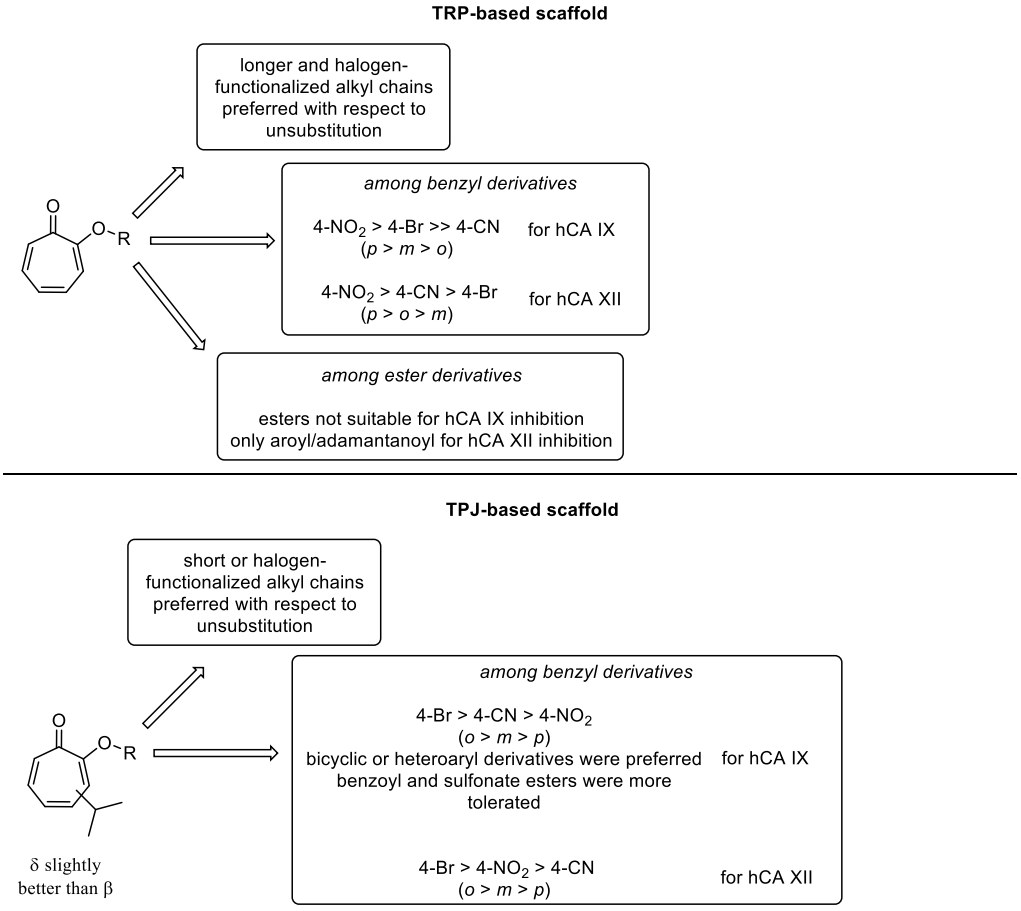

Fig. 4. Main SAR considerations against cancer-related isoforms visualized through substitution patterns.

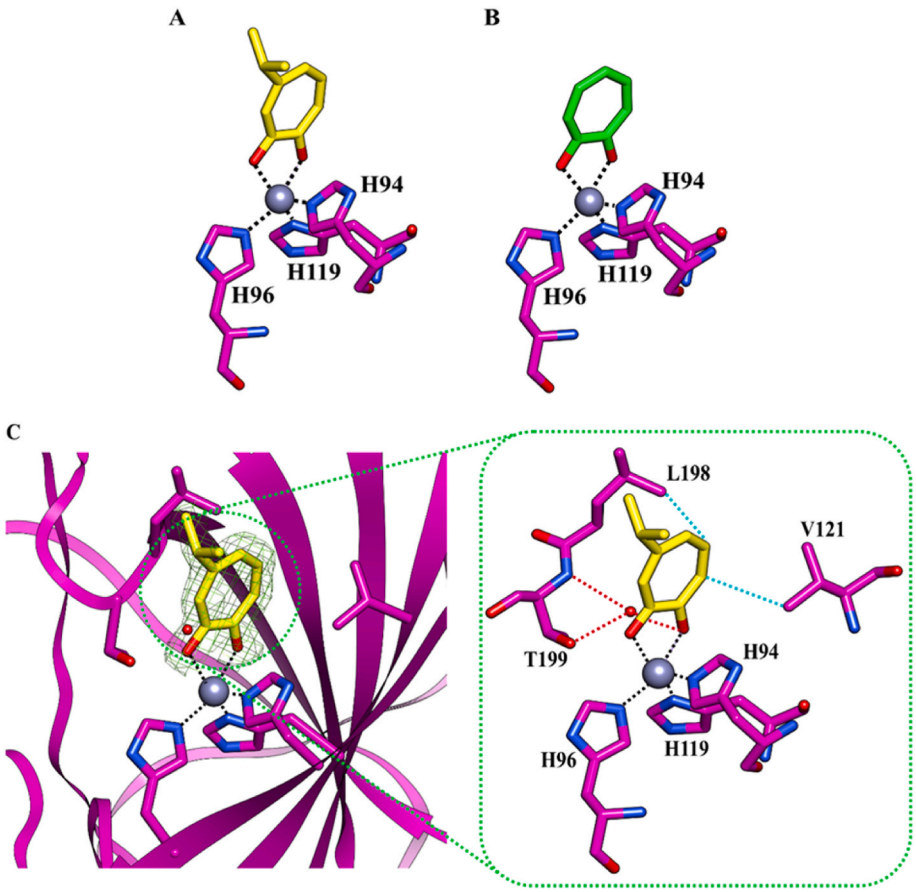

Fig. 5. The structures show the active site of CA II complexed with (**A**) β-**TJP** (PDB ID: 9H0W) and (**B**) **TRP** (PDB ID: 5THJ) [3]. The gray sphere represents the catalytic zinc ion while the coordination bonds are depicted as black dotted lines. (**C**) The active site of hCA II complexed with β-**TJP** (PDB ID: 9H0W). The ligands β-**TJP** and **TRP** are represented in yellow and green sticks, respectively. Residues involved in the binding of the inhibitor are also shown in magenta sticks. Water bridges and hydrophobic interactions are depicted as red and cyan dotted lines whereas coordination interactions are in gray dotted lines. The gray sphere represents the catalytic zinc ion. A |2Fo-Fc| map is shown for the ligand contoured at 1 sigma. (For interpretation of the references to colour in this figure legend, the reader is referred to the Web version of this article.)

sulfonamide inhibiting chemotype (Fig. 5C). Comparing our structure with that of hCA II with **TRP**, which was solved by Dick et al. [3] It is observed that both inhibitors adopt the same orientation and establish analogous interactions within the active site of hCA II (Fig. 5B).

2.5. *In silico investigation on hCAs and tropolonoid derivatives*

Modelling studies were carried out to investigate the binding mode and the energy interaction between the different hCA isoforms and **TRP** and **TJP** derivatives. Regarding the **TJP** derivatives in a mixture the recognition analysis was performed considering both the β-**TJP** and δ-**TJP** regioisomers.

Computational studies revealed that all the compounds are well accommodated in the targets' active site and are associated with a favorable energy interactions profile (data are reported in the Supplementary Material file, Tables S2-S4). In detail, the most active compounds (**1**, **1δ**, **11**, **9**, **8**) on hCA I are accommodated in the catalytic pocket engaging in an H-bond interaction with the Gln92. Interestingly, the 2-nitrobenzyloxy group of compound **11** forms a pi-stacking interaction with Phe91, while compound **8** through the 4-cyanobenzyloxy moiety establishes a pi-stacking interaction with His94 and metal coordination with the zinc ion (data are reported in the Supplementary Material file, Fig. S79).

Among the active compounds on the hCA II, zinc coordination is observed for compounds **2β+δ**, **6**, **4δ**, **9**, and **14β+δ**. The 3-chloropropyl tail of **2β+δ** establishes a halogen bond with Asn62, meanwhile the 4-bromobenzoxy function of **7δ** forms three halogen bond interactions: two with Thr199 and one with Thr200 (Fig. S80). Interestingly, we notice that among the analyzed **TJP** derivatives, compounds **2β+δ**, **4δ**, **7δ**, and **14β+δ** are involved in the same hydrophobic interactions observed in the **TJP**-hCA II crystallographic structure.

For hCA VA, the *p*-tosyl moiety of the most active compound **17δ** establishes a pi-stacking with the Tyr100, and through the carbonyl of β-**TJP** coordinates the metal in the binding site. Moreover, all other active compounds, β-**TJPs**, **2**, **2β+δ**, **6**, **7δ**, **12**, and **11β**, interact with the zinc ion of the binding site (Fig. S81). Furthermore, **6** is also involved in a salt-bridge interaction with Arg282, meanwhile, **11β** is engaged in a salt-bridge with Glu142.

Regarding the isoform VII, the 4-bromobenzyl tail of **7δ**, the most potent molecule in the inhibition of this isoform, establishes a halogen bond with Thr199, a pi-stacking interaction with His94 and an H-bond contact with Gln92. Moreover, the nitro derivative **10β+δ** is involved in the metal coordination and in two H-bond interactions with Gln67 and Thr199 residues (Fig. S82).

Analyzing the most active compounds on the hCA IX isoform we observed that most of them bind to the enzyme active site anchoring themselves to the catalytic zinc ion. Moreover, an interesting network of interactions takes place between ligands and the active site. In detail, the 4-bromobenzyloxy tail of **6δ** forms a halogen bond interaction with Glu106, while the chlorine atom of **2β+δ** forms the same interaction with Tyr11. The naphthyl portion of compound **13δ** is engaged in two

pi-stacking interactions with the imidazole ring of His94. Compounds **8β+δ** and **14β+δ** establish an H-bond interaction with Gln92 and a pi-stacking interaction with His94. Interestingly, **17β** isomer establishes the same interactions of the two last compounds and, in addition, is able to form another hydrogen bond with Thr201. Finally, the nitro derivative compound **11δ** establishes a hydrogen bond with Gln92 and a salt bridge interaction with Glu106 (Fig. 6).

The binding mode of most of the highly active compounds on the hCA XII isoform is characterized by the zinc atom coordination and polar interactions. Specifically, the adamantane derivatives **16** and **16β+δ** interact with the Gln92 via H-bond. The 4-nitrobenzyloxy **TRP9** and the cyano **TRP** derivative **8** are involved in a pi-stacking interaction with His94 and form an H-bond with Thr200. Conversely, **15**, through its nitro group, forms a salt bridge with Lys170 (Fig. 7).

2.6. Antiproliferative effect of representative tropolonoids on multiple myeloma cells

We investigated the antiproliferative activity of representative compounds of the series herein described using, as a model, multiple myeloma (MM), an incurable malignancy characterized by the accumulation of plasma cells in the bone marrow [40]. First, by Western blot we analyzed the protein expression levels of hCA IX and hCA XII in a panel of ten MM cell lines (namely AMO, AMO-BZB, NCI–H929, NCI–H929-BZB, NCI–H929-CFZ, KMS26, KMS26-BZB, MM1S, JJN3, U266) and peripheral blood mononuclear cells (PBMCs) from three different healthy donors. Results indicate that MM cell lines overexpress both hCAs IX and XII compared to healthy PBMCs, and hCA IX levels are overall higher than hCA XII in these cells (Fig. S83A in the Supplementary Material file). Thus, isoenzymes seem to play a crucial role in

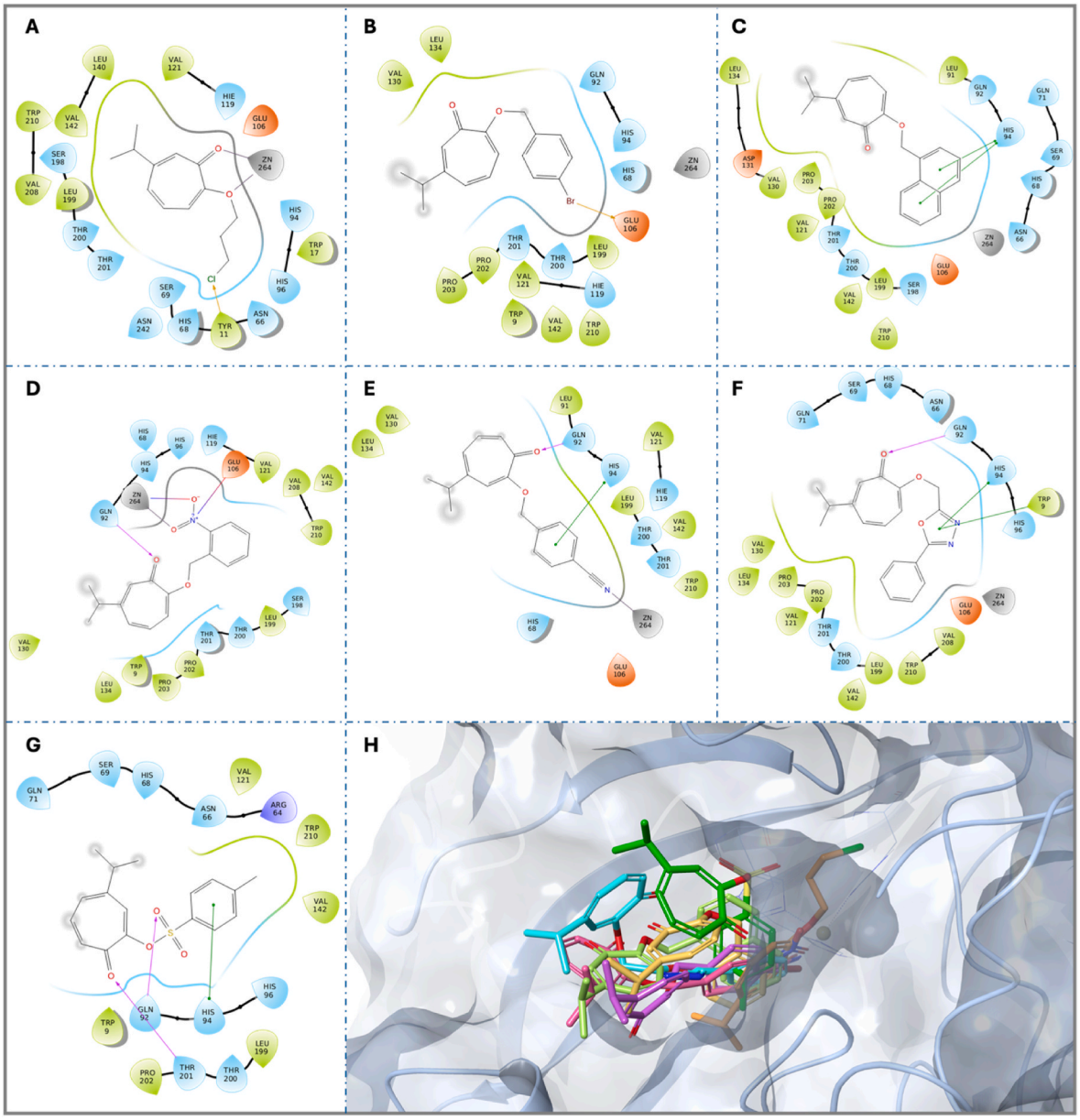

Fig. 6. 2D interaction diagram for compounds **A) 2δ**; **B) 7δ**; **C) 13δ**; **D) 11δ**; **E) 8β**; **F) 14δ**; **G) 17δ** in complex with hCA IX; **H)** shows the superposition of the seven most active compounds **2δ** (orange sticks), **7δ** (violet sticks), **13δ** (light green sticks), **11δ** (light yellow sticks), **8β** (magenta sticks), **14δ** (cyan sticks), and **17β** (green sticks). hCA IX is represented as a slate surface, the zinc ion and the coordinating histidine residues within the active site are shown as a yellow ball and slate sticks, respectively. For derivatives in mixture, the best-scored isomer is shown. (For interpretation of the references to colour in this figure legend, the reader is referred to the Web version of this article.)

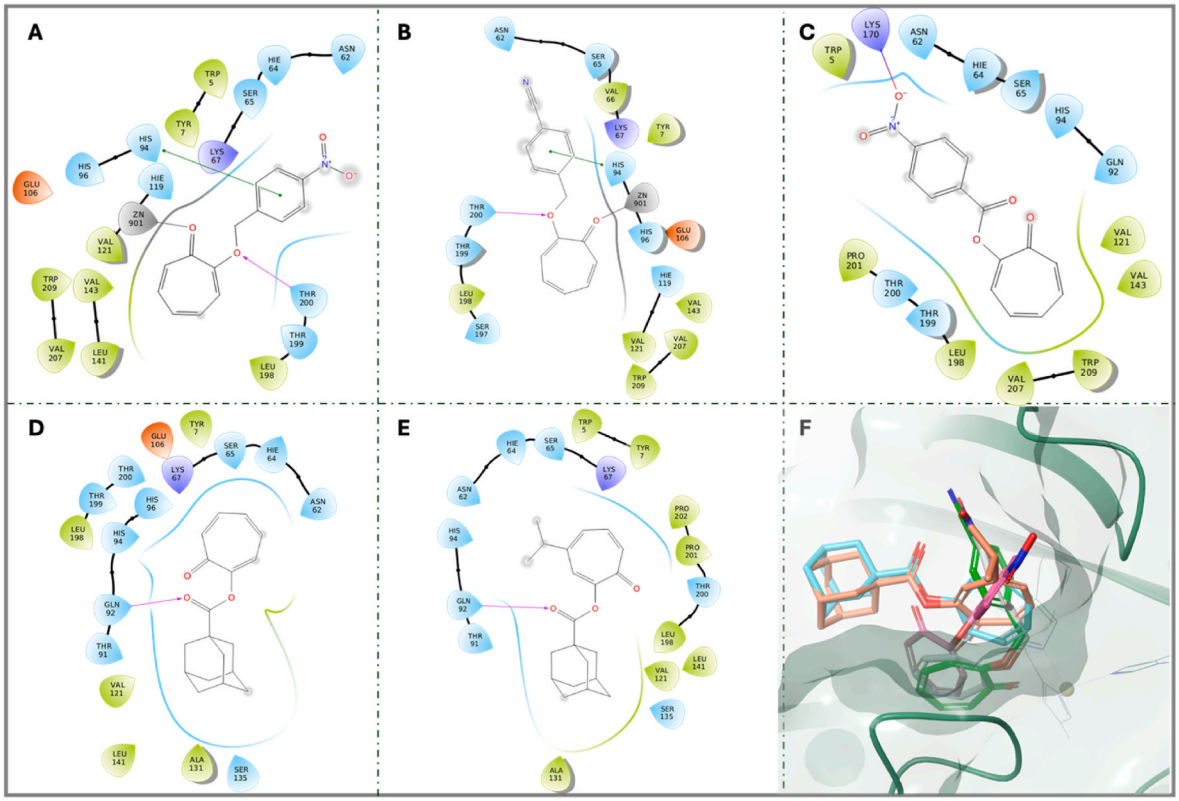

Fig. 7. 2D interaction diagram for **A**) **9**; **B**) **8**; **C**) **15**; **D**) **15**; **E**) **17β** compounds in complex with hCA XII; **F**) shows the superposition of the five most active compounds (**9** in white carbon sticks, **8** (green sticks), **15** (salmon sticks), **15** (cyan sticks), and **17β** (magenta sticks). hCA XII is represented as a forest surface, the zinc ion and the coordinating histidine residues withing the active site are shown as yellow a ball and forest sticks, respectively. For derivatives in mixture the best scored isomer is shown. (For interpretation of the references to colour in this figure legend, the reader is referred to the Web version of this article.)

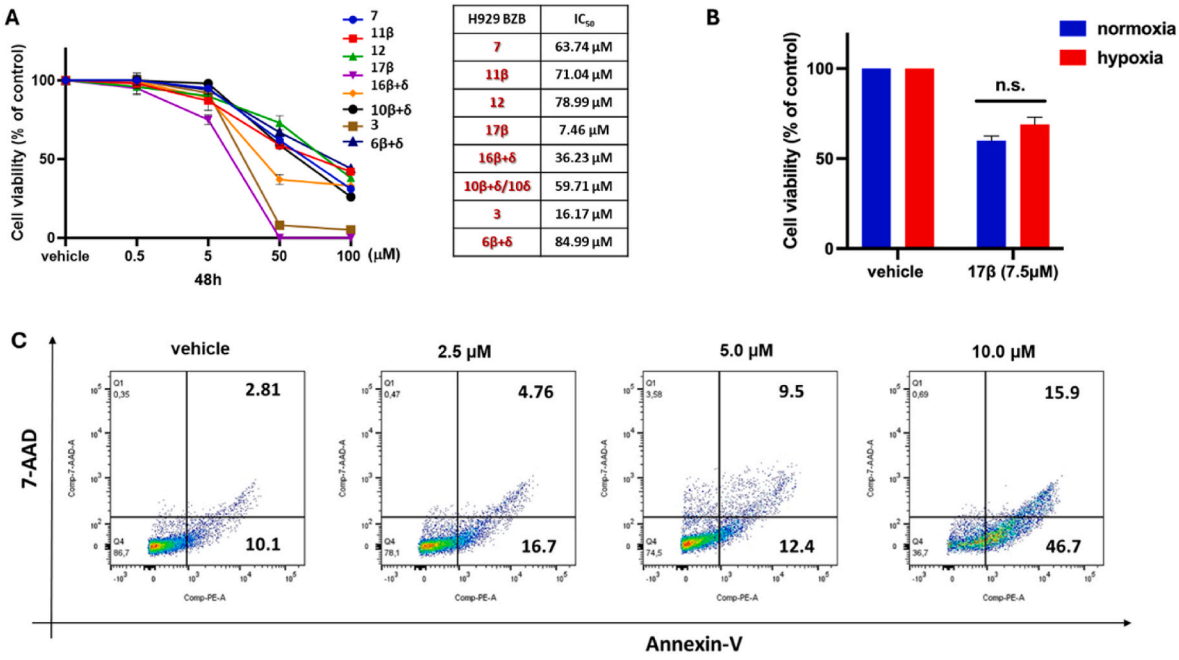

H929 BZB	IC_{50}
7	63.74 μM
11β	71.04 μM
12	78.99 μM
17β	7.46 μM
16β+δ	36.23 μM
10β+δ/10δ	59.71 μM
3	16.17 μM
6β+δ	84.99 μM

Fig. 8. **A**) Cell viability was evaluated using Cell Titer Glo assay (CTG) in H929-BZB cells treated with **TRP** derivatives; IC_{50} values are shown in the associated table. **B**) The viability of H929-BZB cells treated with 7.5 μM **17β** for 48 h, was evaluated under normoxic or hypoxic conditions, using the CTG assay; results are represented as the percentage of viable cells with respect to vehicle (DMSO); n.s.: not significant difference. **C**) Apoptosis was assessed via FACS analysis in H929-BZB treated for 48 h with **17β** at 2.5, 5, and 10 μM or vehicle (DMSO); dot plots show Annexin V-positive cells from independent biological replicates (n = 3). FACS quadrants: Q1, Q2, Q3, and Q4 represent dead cells (7-AAD+), late apoptosis cells (7-AAD + Annexin V+), early apoptosis cells (Annexin V+ 7-AAD−), living cells (7-AAD− Annexin V−), respectively.

the signature of these cells, being putative biomarkers for MM. According to these findings, the development of hCA IX and XII inhibitors could be a suitable and fully exploitable strategy to selectively target MM cells with no detrimental effect on healthy cells displaying low levels of such enzymes. Interesting pieces of information came from three of the investigated cell lines that showed a phenotype resistant to Bortezomib (BZB) (namely AMO-BZB, NCI–H929-BZB, KMS26-BZB) and one to Carfilzomib (CFZ) (namely NCI–H929-CFZ), two proteasome inhibitors. In fact, for most of these cell lines, the levels of hCA isoenzymes, especially hCA IX, seem to be slightly affected by the acquisition of drug resistance.

Thus, we selected NCI–H929-BZB cells to perform the *in vitro* evaluation of the antiproliferative effect for representative compounds (**6β+δ**, **3**, **7**, **12**, **11β**, **10δ**, **15β**, and **17β**). As a result, **17β** emerged as the compound with the lowest IC_{50} value (=7.46 μM, Fig. 8A), even capable of decreasing MM cell survival in hypoxic conditions (Fig. 8B), while sparing healthy PBMCs (Fig. S83B in the Supplementary Material file)

Since H929-BZB cells express high levels of hCA IX while neglectable levels of hCA XII, these data suggest that **17β** exerts anti-tumor activity against MM cell lines, even resistant to standard therapies, mainly via hCA IX inhibition, and can be thus considered *a bona fide* hCA IX inhibitor with low micromolar anti-MM activity. Moreover, FACS analysis indicates that treatment with **17β** can trigger potent pro-apoptotic activity, as demonstrated by the dose-dependent increase in Annexin V/7-AAD staining (Fig. 8C). Altogether, these findings indicate that compound **17β** exerts anti-MM activity with a safe toxicity profile on healthy cells.

2.7. Chemical stability of compound 17β

The presence of the tosyl ester moiety in **17β** prompted us to investigate its chemical stability at the pH values of the enzymatic assay. This was assessed by dissolving the compound in a mixture of DMSO-d_6/D_2O 1/1 *v/v* and monitoring it through ^{1}H NMR spectroscopy at different times (till 120 h). At t_0 (corresponding to the time of compound solubilization in the deuterated solvents and stirring), we could also slightly appreciate the presence of the signals of the two portions of the molecule **17β** after a limited hydrolysis, as evident by observing the aliphatic ppm range, till 120 h (^{1}H NMR overlapped spectra are provided in the Supplementary Material file, Fig. S84). However, further studies through HPLC-MS will be performed to confirm our hypothesis.

3. Conclusions

In agreement with our research interests to identify new scaffolds from natural sources worth investigating and developing for biomedical applications, we report a multidisciplinary study on *O*-substituted troponoloids. Specifically, the naturally occurring **TRP** and β-**TJP** were subjected to *O*-alkyl/acyl or sulfonyl substitutions under basic conditions to afford a large library of compounds that accounted for **TRP** *O*-derivatives and mixtures of β- and δ-**TJP** regioisomers depending on the keto-enolic rearrangement which takes place upon the deprotonation step. Although, in some cases, we were not able to separate the regioisomers resulting from the synthetic pathway, we decided to proceed with biological evaluation also for regioisomer mixtures after identifying the molar ratio they were present in the mixture. Compound regioisomeric structures were assigned by means of multidimensional- and NOESY-NMR experiments before being assessed *in vitro* for their ability to inhibit a panel of physio/pathologically relevant hCAs. Besides the effectiveness of the screened compounds in inhibiting such metalloenzymes along with variegate kinetic trends, it is worth highlighting that the reported K_I values constitute the first CA-directed structure-activity relationship (SAR) dataset on synthetic **TRP**-and **TJP**-*O*-derivatives. We are therefore confident that this work will contribute substantially to the field by giving first-hand structural information necessary to validate troponoloids as a new class of scaffolds endowed with biomedical features.

The binding mode of the natural product β-**TJP** within the hCA II catalytic cleft was assessed by means of X-ray crystallography of the hCA II/β-**TJP** complex. Electron density maps clearly showed bidentate coordination of the ligand with the catalytic Zn(II) ion further assisted by a network of water-bridged hydrogen bonds with the T199 residue, and thus similar to the canonical binding cluster reported for the prototypical CAIs of the sulfonamide type [41]. No relevant differences between hCA II/β-**TJP** and hCA II/**TRP** [3] were spotted also considering that the hydrophobic interactions with L198 and V121 place both ligands with identical orientations within the catalytic cleft.

Based on available experimental data, the binding modes of **TRP** and selected **TJP**-*O*-derivatives were predicted *in silico* on the mitochondrial hCA VA, hCA VII and the tumor-associated IX and XII isoforms. Finally, the selected **17β** isomer was studied for its chemical stability and screened along with other hCA IX/XII selective **TJP** derivatives for antiproliferative activity on multiple myeloma (MM) cell lines. The obtained data strongly indicated **17β** as a potent pro-apoptotic inducer with a safe toxicity profile on healthy cells used as a reference.

However, the bioactivity observed for the mixture of regioisomers is clearly the result of the combined effects of the two regioisomers individual effects, and, at the moment, we have limited knowledge regarding their combination, which could be synergistic, additive, or even antagonistic. However, observing the inhibitory data shown in Table 1, we could assume that no large differences in K_I values are generated by the isolated regioisomers. This seems to suggest that the regioisomerism does not significantly impact the affinity or bioactivity of the compound couples. Nevertheless, to confirm our hypothesis, we are still working on these compounds to gain and test the regioisomers individually, by exploring various separation techniques and regioselective syntheses. Overall, the data reported in our manuscript strongly support troponoloids as a new class of naturally occurring compounds potentially exploitable for biomedical applications by means of appropriate chemical manipulation. Further studies are currently ongoing in this direction.

4. Experimental section

4.1. Chemistry

4.1.1. General chemistry

All commercially available chemicals and solvents were used as purchased. Chromatographic separations were performed on columns packed with silica gel (230–400 mesh, for flash technique). Reactions were monitored through thin-layer chromatography (TLC) performed on 0.2-mm-thick silica gel-aluminum-backed plates (60 F254). TLC spot was visualized under short (254 nm) and long (365 nm) wavelengths ultra-violet irradiation and stained with basic permanganate stains. ^{1}H and ^{13}C NMR were recorded on a Bruker Avance spectrometer operating at 300/400/600 and 75/100/151 MHz, respectively. For compounds **8**, **9**, **11**, **15** and **17**, ^{1}H and ^{13}C NMR were recorded on a Varian Gemini 500 (Palo Alto, CA, USA) spectrometer operating at 500 and 125 MHz, respectively. Spectra are reported in parts per million (δ scale) and internally referenced to the $CDCl_3$, Acetone-d_6, CD_3OD, and DMSO-d_6 signal, respectively at δ 7.26, 2.05, 3.31, and 2.50 ppm. Data are shown as follows: chemical shift, multiplicity (s = singlet, d = doublet, t = triplet, q = quartet, qi = quintet, m = multiplet and/or multiplet resonances, br = broad signal), integration and coupling constants (*J*) in Hertz (Hz). Chemical shifts for carbon are reported in parts per million (*δ* scale) and referenced to the carbon resonances of the solvent ($CDCl_3$ at δ 77.0, CD_3OD at δ 49.0, and DMSO-d_6 at δ 39.0 ppm). Melting points were measured on a Stuart® melting point apparatus SMP3 (Merck s.r.l., Milan, Italy) and are uncorrected (temperatures are reported in °C). Elemental analyses for C, H, and N were recorded on a PerkinElmer 240 B microanalyzer and the analytical results were within ±0.4% of the

theoretical values for all compounds.

4.1.2. Synthetic procedures and characterization data for derivatives 1-16

4.1.2.1. General procedure for the synthesis of compounds 13, 7-14. Potassium carbonate (4.0 equivalents) was added in a solution of **TRP** or **TJP** (1.0 equivalent) and the proper halide (1.5 equivalents for the alkyl halides, whereas 3.0 equivalents for benzyl ones) in refluxing acetonitrile (0.4 M). Then, the reaction mixture was poured into an oversaturated aqueous solution of Na_2CO_3 and extracted with DCM three times. The combined organic layers were dried over sodium sulfate anhydrous, filtered, and evaporated *in vacuo* to obtain the crude product. The compounds were purified through flash column chromatography, employing silica gel and the suitable eluent (i.e., *n*-hexane/ethyl acetate, *n*-hexane/diethyl ether, DCM/MeOH).

2-(prop-2-yn-1-yloxy)cyclohepta-2,4,6-trienone (1). Orangish solid; m.p. 88–89 °C; 54 % yield. **^{1}H NMR** (600 MHz, $CDCl_3$): δ 2.54 (t, J = 2.4 Hz, 1H, C ≡ CH), 4.88 (s, 2H, OCH_2), 6.90 (dddd, J = 10.8, 5.3, 3.9, 0.8 Hz, 1H, Ar), 6.96 (d, J = 9.8 Hz, 1H, Ar), 7.03–7.10 (m, 1H, Ar), 7.21–7.24 (m, 2H, Ar). **^{13}C NMR** (151 MHz, $CDCl_3$) δ 56.7, 115.8, 129.2, 132.4, 138.0, 163.2. Anal. calcd for $C_{10}H_8O_2$: C, 74.99; H, 5.03. Found: C, 74.84; H, 5.09. Characterization data are in agreement with the previous literature [42,43].

4-isopropyl-2-(prop-2-yn-1-yloxy)cyclohepta-2,4,6-trienone (1β+δ). β:δ ratio assessed by ^{1}H NMR analysis: 55:45. The reported IUPAC name is referred to as the β isomer. Black-brown oil; 49 % yield. **^{1}H NMR** (600 MHz, $CDCl_3$): δ 1.28 (d, J = 12.0 Hz, 6H, CH_3 iPro), 1.33 (d, J = 12.0 Hz, 6H, CH_3 iPro), 2.61–2.62 (m, 2H, 2 x C ≡ CH), 2.89–2.93 (m, 2H, 2 x CH iPro), 4.92 (d, J = 6.0 Hz, 2H, OCH_2), 4.96 (d, J = 6.0 Hz, 2H, OCH_2), 6.86–6.88 (m, 1H, Ar), 6.90–6.91 (m, 1H, Ar), 6.94 (s, 1H, Ar), 7.03–7.08 (m, 2H, Ar), 7.15–7.32 (m, 3H, Ar). **^{13}C NMR** (75 MHz, $CDCl_3$): δ 22.0, 22.2, 38.3, 38.9, 56.4, 76.6, 76.8, 114.7, 117.8, 125.9, 130.6, 131.2, 135.1, 135.9, 136.9, 153.9, 157.6, 162.1, 162.4, 180.3. Anal. calcd for $C_{13}H_{14}O_2$: C, 77.20; H, 6.98. Found: C, 77.14; H, 7.01.

2-(3-chloropropoxy)cyclohepta-2,4,6-trienone (2). Orange oil; 86 % yield. **^{1}H NMR** (300 MHz, $CDCl_3$): δ 2.70 (qi, 2H, CH_2), 3.80 (q, 2H, $ClCH_2$), 4.20 (t, J = 6.15 Hz, 2H, OCH_2), 6.77–6.90 (m, 2H, Ar), 7.03–7.06 (m, 1H, Ar), 7.22–7.40 (m, 2H, Ar). **^{13}C NMR** (75 MHz, $CDCl_3$): δ 31.6, 41.4, 65.7, 114.1, 128.5, 133.0, 136.8, 137.2, 164.8, 180.3. Anal. calcd for $C_{10}H_{11}ClO_2$: C, 60.46; H, 5.58. Found: C, 60.53; H, 5.61.

2-(3-chloropropoxy)-4-isopropylcyclohepta-2,4,6-trienone (2β+δ). β:δ ratio assessed by ^{1}H NMR analysis: 50:50. The reported IUPAC name is referred to as the β isomer. Yellow oil; 57 % yield. **^{1}H NMR** (300 MHz, $CDCl_3$): δ 1.73 (d, J = 6.9 Hz, 6H, CH_3 iPro), 1.77 (d, J = 6.3 Hz, 6H, CH_3 iPro), 2.84–2.89 (m, 4H, 2 x CH_2), 3.26–3.37 (m, 2H, 2 x CH iPro), 4.30 (q, 4H, 2 x $ClCH_2$), 4.66–4.75 (m, 4H, 2 x OCH_2), 7.18–7.33 (m, 3H, Ar), 7.50 (q, 1H, Ar), 7.65–7.82 (m, 4H, Ar). **^{13}C NMR** (75 MHz, $CDCl_3$): δ 23.6, 24.0, 32.2, 32.3, 38.9, 39.5, 42.0, 66.0, 113.5, 116.3, 122.8, 125.7, 128.2, 130.2, 132.3, 135.1, 135.7, 137.6, 137.8, 154.9, 158.3, 164.6, 180.6. Anal. calcd for $C_{13}H_{17}ClO_2$: C, 64.86; H, 7.12. Found: C, 64.81; H, 7.09.

2-((5-bromopentyl)oxy)cyclohepta-2,4,6-trienone (3). Yellow oil; 21 % yield. **^{1}H NMR** (300 MHz, Acetone-d_6/$CDCl_3$ mixture to improve solubility): δ 1.48–1.63 (m, 2H, CH_2), 1.85–1.98 (qi, 4H, CH_2), 3.24 (t, J = 6.2 Hz, 2H, CH_2Cl), 4.03 (t, J = 6.2 Hz, 2H, OCH_2), 6.72 (d, J = 9.9 Hz, 1H, Ar), 6.78–6.84 (m, 1H, Ar), 7.03 (t, J = 10.2 Hz, 1H, Ar), 7.08–7.11 (m, 2H, Ar). **^{13}C NMR** (75 MHz, Acetone/$CDCl_3$ mixture to improve solubility): δ 24.7, 27.9, 32.3, 33.5, 69.0, 113.2, 127.8, 132.6, 136.3, 137.1, 180.6. Anal. calcd for $C_{12}H_{15}BrO_2$: C, 53.16; H, 5.58. Found: C, 53.11; H, 5.55.

2-((4-bromobenzyl)oxy)cyclohepta-2,4,6-trienone (7). Pale yellow solid; m.p. 99–101 °C; 55 % yield. **^{1}H NMR** (600 MHz, $CDCl_3$): δ 5.18 (s, 2H, OCH_2), 6.70–6.77 (m, 1H, Ar), 6.84 (dddd, J = 10.8, 7.0, 2.2, 0.6 Hz, 1H, Ar), 6.96 (ddt, J = 10.8, 9.7, 1.0 Hz, 1H, Ar), 7.25–7.18 (m, 2H, Ar), 7.30 (d, J = 8.7 Hz, 1H, Ar), 7.49 (d, J = 8.4 Hz, 1H, Ar). **^{13}C NMR** (151 MHz, $CDCl_3$) δ 70.2, 115.1, 122.3, 128.6, 128.9, 132.0, 132.5, 134.5, 136.5, 137.7, 164.3, 180.8. Anal. calcd for $C_{14}H_{11}BrO_2$: C, 57.76; H, 3.81. Found: C, 57.84; H, 3.86.

2-((4-bromobenzyl)oxy)-6-isopropylcyclohepta-2,4,6-trienone (7δ). Pale red solid; m.p. 76–77 °C; 52 % yield. **^{1}H NMR** (400 MHz, $CDCl_3$): δ 1.21 (d, J = 12.0 Hz, 6H, CH_3 iPro), 2.74–2.79 (qi, 1H, CH iPro), 5.17 (s, 2H, OCH_2), 6.62 (d, J = 12.0 Hz, 1H, Ar), 6.74–6.92 (m, 2H, Ar), 7.19 (s, 1H, Ar), 7.25–7.31 (m, 2H, Ar), 7.49 (d, J = 10.0 Hz, 2H, Ar). **^{13}C NMR** (75 MHz, $CDCl_3$): δ 22.0, 37.7, 71.8, 118.6, 122.0, 124.6, 129.3, 131.8, 135.1, 136.0, 136.4, 153.9, 164.9, 180.5. Anal. calcd for $C_{17}H_{17}BrO_2$: C, 61.28; H, 5.14. Found: C, 61.36; H, 5.11.

4-{ [(7-Oxocyclohepta-1,3,5-trien-1-yl)oxy] methyl}benzonitrile (8). Off-white powder; m.p. 143–145 °C; 48 % yield. **^{1}H NMR** (500 MHz, DMSO-d_6): 5.27 (s, 2H, OCH_2), 6.94 (dd, J = 10.6 Hz and 8.4 Hz, 1H, Ar), 7.04–7.06 (m, 2H, Ar), 7.12–7.16 (m, 1H, Ar), 7.29–7.33 (m, 1H, Ar), 7.64 (d, J = 7.8 Hz, 2H, Ar), 7.87 (d, J = 7.8 Hz, 2H, Ar). **^{13}C NMR** (125 MHz, DMSO-d_6): δ 67.5, 115.3, 125.4, 128.9, 129.6, 129.7, 132.2, 133.6, 134.7, 137.1, 147.5, 163.8, 179.6. Characterization data are in agreement with the previous literature [44].

4-(((3-isopropyl-7-oxocyclohepta-1,3,5-trien-1-yl)oxy)methyl) benzonitrile (8β+δ). β:δ ratio assessed by ^{1}H NMR analysis: 50:50. The reported IUPAC name is referred to as the β isomer. Brownish oil; 70 % yield. **^{1}H NMR** (600 MHz, $CDCl_3$): δ 1.15 (d, J = 7.0 Hz, 6H, CH_3 iPro), 1.23 (d, J = 6.6 Hz, 6H, CH_3 iPro), 2.71–2.79 (m, 2H, 2 x CH iPro), 5.26 (s, 2H, OCH_2), 5.31 (s, 2H, OCH_2), 6.64 (d, J = 9.5 Hz, 2H, Ar), 6.70 (s, 2H, Ar), 6.79 (d, J = 8.8 Hz, 2H, Ar), 6.81 (dd, J = 11.4, 1.5 Hz, 2H, Ar), 6.92 (dd, J = 11.2, 9.7 Hz, 2H, Ar), 7.12 (d, J = 11.4 Hz, 2H, Ar), 7.19 (dd, J = 12.1, 8.8 Hz, 2H, Ar), 7.19 (d, J = 1.5 Hz, 2H, Ar), 7.57 (d, J = 8.1 Hz, 2H, Ar), 7.59 (d, J = 8.4 Hz, 2H, Ar), 7.67 (d, J = 6.6 Hz, 2H, Ar), 7.68 (d, J = 7.0 Hz, 2H, Ar). **^{13}C NMR** (151 MHz, $CDCl_3$): δ 23.0, 23.1, 38.3, 38.7, 69.5, 69.7, 112.0, 114.3, 117.6, 118.5, 118.5, 125.8, 127.4, 127.4, 130.4, 131.1, 132.5, 135.0, 135.8, 136.9, 141.0, 141.2, 153.6, 157.6, 162.9, 163.1, 180.1, 180.2. Anal. calcd for $C_{18}H_{17}NO_2$: C, 77.40; H, 6.13; N, 5.01. Found: C, 77.49; H, 6.16; N, 5.08.

2-((4-Nitrobenzyl)oxy)cyclohepta-2,4,6-trien-1-one (9). Off-white powder; m.p. 164–166 °C; 48 % yield. **^{1}H NMR** (500 MHz, DMSO-d_6): 5.33 (s, 2H, OCH_2), 6.92–6.94 (m, 1H, Ar), 7.05–7.07 (m, 2H, Ar), 7.13–7.17 (m, 1H, Ar), 7.30–7.32 (m, 1H, Ar), 7.71 (d, J = 8.2 Hz, 2H, Ar), 8.26 (d, J = 8.2 Hz, 2H, Ar). **^{13}C NMR** (125 MHz, DMSO-d_6): δ 69.2, 115.2, 124.1, 128.7, 128.9, 133.4, 137.1, 137.2, 144.3, 147.6, 163.9, 179.7. Characterization data are in agreement with the previous literature [45].

4-isopropyl-2-((4-nitrobenzyl)oxy)cyclohepta-2,4,6-trienone (9β+δ). β:δ ratio assessed by ^{1}H NMR analysis: 50:50. The reported IUPAC name is referred to as the β isomer. Orange solid; m.p. 92–94 °C; 75 % yield. **^{1}H NMR** (400 MHz, $CDCl_3$): 1.16 (d, J = 8.0 Hz, 6H, CH_3 iPro), 1.24 (d, J = 8.0 Hz, 6H, CH_3 iPro), 2.74–2.82 (m, 2H, 2 x CH iPro), 5.30 (s, 2H, OCH_2), 5.35 (s, 2H, OCH_2), 6.66 (d, J = 8.0 Hz, 1H, Ar), 6.73 (s, 1H, Ar), 6.81 (t, J = 8.0 Hz, 2H, Ar), 6.92 (t, J = 9.7 Hz, 1H, Ar), 7.13–7.25 (m, 3H, Ar), 7.64 (t, J = 8.9 Hz, 4H, Ar), 8.24 (dd, J = 7.1, 4.1 Hz, 4H, Ar). **^{13}C NMR** (75 MHz, $CDCl_3$): δ 23.0, 23.2, 38.4, 38.7, 69.4, 69.5, 114.5, 117.8, 124.0, 125.9, 127.5, 127.6, 130.6, 131.1, 135.1, 136.0, 137.0, 143.0, 143.2, 153.7, 157.7, 162.9, 180.1, 180.2. Anal. calcd for $C_{17}H_{17}NO_4$: C, 68.22; H, 5.72; N, 4.68. Found: C, 68.28; H, 5.74; N, 4.63.

2-((3-nitrobenzyl)oxy)cyclohepta-2,4,6-trienone (10). Pale pink solid; m.p. 130–132 °C; 77 % yield. **^{1}H NMR** (400 MHz, $CDCl_3$): δ 5.30 (s, 2H, OCH_2), 6.81 (d, J = 9.8 Hz, 1H, Ar), 6.85–6.97 (m, 1H, Ar), 7.02 (t, J = 8.1 Hz, 1H, Ar), 7.25 (m, 2H, Ar), 7.59 (t, J = 8.0 Hz, 1H, Ar), 7.86 (d, J = 7.7 Hz, 1H, Ar), 8.20 (d, J = 7.8 Hz, 1H, Ar), 8.29 (s, 1H, Ar). **^{13}C NMR** (100 MHz, $CDCl_3$): δ 64.1, 110.0, 115.0, 121.6, 122.8, 128.6, 129.4, 131.8, 132.8, 136.0, 137.2, 137.4, 163.4, 180.0. Anal. calcd for $C_{14}H_{11}NO_4$: C, 65.37; H, 4.31; N, 5.45. Found: C, 65.42; H, 4.35; N, 5.49.

4-isopropyl-2-((3-nitrobenzyl)oxy)cyclohepta-2,4,6-trienone

(10β+δ). β:δ ratio assessed by ^{1}H NMR analysis: 50:50. The reported IUPAC name is referred to as the β isomer. Yellow oil; 39 % yield. **^{1}H NMR** (600 MHz, $CDCl_3$): δ 1.18 (d, *J* = 7.0 Hz, 6H, CH_3 iPro), 1.24 (d, *J* = 6.6 Hz, 6H, CH_3 iPro), 2.75–2.82 (m, 2H, 2 x CH iPro), 5.29 (s, 2H, OCH_2), 5.34 (s, 2H, OCH_2), 6.73 (d, *J* = 9.9 Hz, 1H, Ar), 6.80 (s, 1H, Ar), 6.80 (d, *J* = 10.0 Hz, 1H, Ar), 6.82 (dd, *J* = 11.0, 1.5 Hz, 1H, Ar), 6.95 (dd, *J* = 11.0, 9.9 Hz, 1H, Ar), 7.12 (d, *J* = 12.5 Hz, 1H, Ar), 7.19 (d, *J* = 3.6 Hz, 1H, Ar) 7.19 (t, *J* = 10.3 Hz, 1H, Ar), 7.56–7.60 (m, 2H, Ar), 7.84 (d, *J* = 7.7 Hz, 1H, Ar), 7.87 (d, *J* = 7.7 Hz, 1H, Ar), 8.14–8.16 (m, 2H, Ar), 8.29 (t, *J* = 1.0, 1H, Ar), 8.33 (t, *J* = 1.0, 1H, Ar). **^{13}C NMR** (151 MHz, $CDCl_3$): δ 23.0, 23.2, 38.3, 38.7, 69.5, 69.6, 114.6, 118.0, 122.1, 122.2, 123.2, 125.9, 129.9, 130.5, 131.3, 133.3, 133.4, 135.0, 135.9, 137.0, 137.8, 138.1, 148.4, 153.8, 157.6, 163.0, 163.2, 180.1, 180.2. Anal. calcd for $C_{17}H_{17}NO_4$: C, 68.22; H, 5.72; N, 4.68. Found: C, 68.29; H, 5.68; N, 4.73.

2-((2-Nitrobenzyl)oxy)cyclohepta-2,4,6-trien-1-one (11). Off-white powder; m.p. 151–153 °C; 43 % yield. **^{1}H NMR** (500 MHz, DMSO-d_6): 5.52 (s, 2H, OCH_2), 6.96 (dd, *J* = 10.4 Hz and 8.2 Hz, 1H, Ar), 7.06–7.09 (m, 2H, Ar), 7.14–7.18 (m, 1H, Ar), 7.30–7.32 (m, 1H, Ar), 7.63–7.64 (m, 1H, Ar), 7.88–7.88 (m, 2H, Ar), 8.14–8.16 (dd, 1H, *J* = 8.2 Hz and 1.1 Hz, 1H, Ar). **^{13}C NMR** (125 MHz, DMSO-d_6): δ 67.5, 115.3, 125.4, 128.9, 129.6, 129.7, 132.2, 133.5, 134.7, 137.1, 137.2, 147.5, 163.8, 179.6. Characterization data are in agreement with the previous literature [44].

4-isopropyl-2-((2-nitrobenzyl)oxy)cyclohepta-2,4,6-trienone (11β). Yellow solid; m.p. 139–141 °C; 52 % yield. **^{1}H NMR** (600 MHz, $CDCl_3$): δ 1.19 (d, *J* = 6.6 Hz, 6H, CH_3 iPro), 2.78–2.80 (m, 1H, CH_3 iPro), 5.62 (s, 2H, OCH_2), 6.76 (s, 1H, Ar), 6.80 (d, *J* = 8.4 Hz, 1H, Ar), 7.15 (d, *J* = 12.1 Hz, 1H, Ar), 7.20 (dd, *J* = 12.5, 8.4 Hz, 1H, Ar), 7.51 (td, *J* = 7.8, 0.8 Hz, 1H, Ar), 7.73 (td, *J* = 7.6, 1.1 Hz, 1H, Ar), 8.10 (d, *J* = 7.7 Hz, 1H, Ar), 8.19 (dd, *J* = 8.1, 1.1 Hz, 1H, Ar). **^{13}C NMR** (151 MHz, $CDCl_3$): δ 23.2, 38.8, 67.4, 117.0, 125.0, 125.6, 128.6, 128.9, 132.6, 134.5, 135.7, 137.0, 146.6, 154.0, 163.0, 180.1. Anal. calcd for $C_{17}H_{17}NO_4$: C, 68.22; H, 5.72; N, 4.68. Found: C, 68.13; H, 5.67; N, 4.74. Characterization data are in agreement with the previous literature [26].

6-isopropyl-2-((2-nitrobenzyl)oxy)cyclohepta-2,4,6-trienone (11δ). Yellow solid; m.p. 139–140 °C; 31 % yield. **^{1}H NMR** (600 MHz, $CDCl_3$): δ 1.24 (d, *J* = 6.8 Hz, 6H, CH_3 iPro), 2.76–2.81 (m, 1H, CH_3 iPro), 5.58 (s, 2H, OCH_2), 6.71 (d, *J* = 9.5 Hz, 1H, Ar), 6.82 (dt, *J* = 11.0 Hz, 1H, Ar), 6.96 (ddd, *J* = 11.2, 10.2, 1.2 Hz, 1H, Ar), 7.21 (s, 1H, Ar), 7.50 (t, *J* = 7.9 Hz, 1H, Ar), 7.72 (t, *J* = 7.5 Hz, 1H, Ar), 8.08 (d, *J* = 8.1 Hz, 1H, Ar), 8.20 (d, *J* = 8.1 Hz, 1H, Ar). **^{13}C NMR** (151 MHz, $CDCl_3$): δ 23.0, 38.4, 67.4, 113.9, 125.0, 128.6, 128.7, 130.3, 131.4, 132.6, 134.6, 134.9, 146.4, 157.6, 163.2, 180.2. Anal. calcd for $C_{17}H_{17}NO_4$: C, 68.22; H, 5.72; N, 4.68. Found: C, 68.27; H, 5.76; N, 4.73.

2-((3-(trifluoromethyl)benzyl)oxy)cyclohepta-2,4,6-trienone (12). Pale pink solid; m.p. 99–100 °C; 58 % yield. **^{1}H NMR** (300 MHz, $CDCl_3$): δ 5.22 (s, 2H, OCH_2), 6.76–7.03 (m, 3H, Ar), 7.23–7.26 (m, 2H, Ar), 7.48–7.7.67 (m, 4H, Ar). **^{13}C NMR** (75 MHz, $CDCl_3$): δ 70.1, 115.2, 123.9, 125.1, 125.1, 128.7, 129.3, 130.6, 132.2, 136.4, 136.5, 137.7, 164.1, 180.6. Anal. calcd for $C_{15}H_{11}F_3O_2$: C, 64.29; H, 3.96. Found: C, 64.33; H, 3.91.

4-isopropyl-2-((3-(trifluoromethyl)benzyl)oxy)cyclohepta-2,4,6-trienone (12β). Orange oil; 31 % yield. **^{1}H NMR** (400 MHz, $CDCl_3$): δ 1.15–1.22 (m, 6H, CH_3 iPro), 2.75–2.87 (m, 1H, CH iPro), 5.38 (s, 2H, OCH_2), 6.77–6.90 (m, 2H, Ar), 7.22 (t, *J* = 3.7 Hz, 2H, Ar), 7.57 (t, *J* = 7.4 Hz, 1H, Ar), 7.65 (d, *J* = 7.4 Hz, 1H, Ar), 7.74 (d, *J* = 8.7 Hz, 2H, Ar). **^{13}C NMR** (100 MHz, $CDCl_3$): δ 23.1, 38.8, 70.2, 117.6, 123.9, 124.0, 125.1, 125.7, 129.4, 130.6, 135.8, 136.9, 138.7, 153.8, 163.1, 180.3. Anal. calcd for $C_{18}H_{17}F_3O_2$: C, 67.07; H, 5.32. Found: C, 67.00; H, 5.29.

6-isopropyl-2-((3-(trifluoromethyl)benzyl)oxy)cyclohepta-2,4,6-trienone (12δ). Orange oil; 36 % yield. **^{1}H NMR** (400 MHz, $CDCl_3$): δ 1.26 (tt, *J* = 6.7, 3.6 Hz, 6H, CH_3 iPro), 2.81 (quint, 1H, CH iPro), 5.28 (s, 2H, OCH_2), 6.72 (d, *J* = 9.7 Hz, 1H, Ar), 6.83 (d, *J* = 11.2, 1H, Ar), 6.96 (t, *J* = 10.5 Hz, 1H, Ar), 7.53 (t, *J* = 7.8 Hz, 1H, Ar), 7.61 (d, *J* = 8.0 Hz, 1H, Ar), 7.66–7.44 (m, 2H, Ar). **^{13}C NMR** (75 MHz, $CDCl_3$): δ 22.0, 38.4, 70.0, 114.3, 123.9, 123.9, 125.0, 125.1, 129.3, 130.3, 131.2, 135.0, 136.6, 157.6, 163.4, 180.3. Anal. calcd for $C_{18}H_{17}F_3O_2$: C, 67.07; H, 5.32. Found: C, 67.16; H, 5.36.

2-(naphthalen-1-ylmethoxy)cyclohepta-2,4,6-trienone (13). Orange solid; m.p. 116–117 °C; 75 % yield. **^{1}H NMR** (300 MHz, $CDCl_3$): δ 5.65 (s, 2H, OCH_2), 6.84–6.60 (m, 3H, Ar), 7.23 (t, *J* = 6.5 Hz, 2H, Ar), 7.42–7.62 (m, 4H, Ar), 7.82–7.91 (m, 2H, Ar), 8.04 (d, *J* = 7.8 Hz, 1H, Ar). **^{13}C NMR** (75 MHz, $CDCl_3$) δ 69.5, 115.4, 123.1, 125.3, 126.0, 126.0, 126.6, 128.4, 128.8, 129.0, 130.6, 131.0, 132.5, 133.7, 136.3, 137.6, 164.6, 180.7. Anal. calcd for $C_{18}H_{14}O_2$: C, 82.42; H, 5.38. Found: C, 82.46; H, 5.42.

6-isopropyl-2-(naphthalen-1-ylmethoxy)cyclohepta-2,4,6-trienone (13δ). Pale red solid; m.p. 93–94 °C; 52 % yield. **^{1}H NMR** (400 MHz, $CDCl_3$): δ 1.23 (d, *J* = 12.0 Hz, 6H, CH_3 iPro), 2.75–2.79 (m, 1H, CH iPro), 5.68 (s, 2H, OCH_2), 7.75 (d, *J* = 9.0 Hz, 1H, Ar), 6.84–6.88 (m, 1H, Ar), 7.21 (s, 1H, Ar), 7.41–7.60 (m, 4H, Ar), 7.81–7.90 (dd, *J* = 13.4, 12.0 Hz, 2H, Ar), 8.04 (d, *J* = 12.0 Hz, 1H, Ar). **^{13}C NMR** (75 MHz, $CDCl_3$): δ 23.0, 38.3, 69.3, 114.5, 123.2, 125.3, 126.0, 126.6, 128.8, 128.9, 129.9, 130.7, 131.0, 131.4, 133.7, 134.9, 157.3, 163.9, 180.5. Anal. calcd for $C_{21}H_{20}O_2$: C, 82.86; H, 6.62. Found: C, 82.92; H, 6.66.

4-isopropyl-2-((5-phenyl-1,3,4-oxadiazol-2-yl)methoxy)cyclohepta-2,4,6-trienone (14β+δ). β:δ ratio assessed by ^{1}H NMR analysis: 50:50. The reported IUPAC name is referred to as the β isomer. Brownish oil; yield 30 %. **^{1}H NMR** (300 MHz, DMSO-d_6): δ 1.14–1.18 (m, 12H, 2 x CH_3 iPro), 2.72–2.88 (m, 2H, 2 x CH iPro), 5.52 (s, 2H, OCH_2), 5.62 (s, 2H, OCH_2), 6.90–6.97 (m, 4H, Ar), 7.08–7.11 (m, 3H, Ar), 7.27 (dd, *J* = 12.3, 9.0 Hz, 1H, Ar), 7.57–7.65 (m, 6H, Ar), 7.98–8.01 (m, 4H, Ar). **^{13}C NMR** (75 MHz, DMSO-d_6): δ 25.9, 26.1, 42.3, 42.6, 64.3, 120.5, 123.5, 127.0, 130.6, 131.2, 131.3, 132.3, 133.0, 135.5, 136.1, 136.5, 138.1, 139.0, 142.6, 159.6, 164.1, 166.0, 166.1, 166.3, 166.4, 170, 184.2. Anal. calcd for $C_{19}H_{18}N_2O_3$: C, 70.79; H, 5.63, N, 8.69. Found: C, 70.72; H, 5.60, N, 8.75.

4.1.3. Synthesis of derivative 4δ

7,7'-(pentane-1,5-diylbis(oxy))bis(3-isopropylcyclohepta-2,4,6-trienone) (4δ). Potassium carbonate (4.0 equivalents) was added in a solution of β-**TJP** (2.0 equivalents) and 1,5-dibromopentane (1.0 equivalent for the alkyl halides, whereas 3.0 equivalents for benzyl ones) in refluxing acetonitrile (0.4 M). Then, the reaction mixture was poured into an oversaturated aqueous solution of Na_2CO_3 and extracted with DCM three times. The combined organic layers were dried over sodium sulfate anhydrous, filtered, and evaporated *in vacuo* to obtain the crude product. The compound was purified through flash column chromatography, employing silica gel and a mixture of 5% MeOH in 95% DCM as mobile phase.

Orangish oil; 19 % yield. **^{1}H NMR** (300 MHz, $CDCl_3$): δ 1.22 (d, *J* = 3.0 Hz, 6H, CH_3 iPro), 1.25 (d, *J* = 3.0 Hz, 6H, CH_3 iPro), 1.54–1.76 (m, 2H, CH iPro), 1.54–1.70 (m, 4H, 2 x CH_2), 1.96–2.01 (m, 3H, CH_2), 2.73–2.77 (m, 2H, CH iPro), 2.81–2.83 (m, 1H, CH iPro), 4.02–4.10 (m, 3H, OCH_2), 6.61–6.64 (m, 1H, Ar), 6.68 (m, 1H, Ar), 6.73–6.77 (m, 2H, Ar), 6.96 (m, 1H, Ar), 7.07–7.09 (m, 1H, Ar), 7.12–7.16 (m, 2H, Ar). **^{13}C NMR** (75 MHz, $CDCl_3$): δ 22.7, 23.2, 23.5, 28.2, 28.3, 28.4, 29.8, 32.3, 38.4, 39.1, 62.6, 69.0, 112.6, 115.2, 124.7, 129.3, 131.8, 134.5, 135.2, 136.9, 154.4, 157.6, 164.3, 164.4, 180.2, 180.4. Anal. calcd for $C_{25}H_{32}O_4$: C, 75.73; H, 8.13. Found: C, 75.80; H, 8.16.

4.1.4. Synthesis of derivatives 6 and 6β+δ

Ethyl bromoacetate (1.5 equivalents) was added to a mixture of **TRP** (1.0 equivalent) for **5** or **TJP** (1.0 equivalent) for **5β+δ** and K_2CO_3 (2.0 equivalents) in acetonitrile (0.4 M). The suspension was allowed to reflux overnight. Then, the reaction mixture was poured into an oversaturated aqueous solution of Na_2SO_4 and extracted with DCM three times. The combined organic layers were dried over anhydrous sodium sulfate, filtered and evaporated under reduced pressure. Both

intermediates were purified through column chromatography, with a mixture of *n*-hexane/ethyl acetate 97:3. To reach compounds **6** and **6β+δ**, **5** (1.0 equivalent) or **5β+δ** (1.0 equivalent) was dissolved in THF (0.12 M), whereas lithium hydroxide monohydrate (LiOH x H_2O) was dissolved in water (0.5 M). The aqueous solution was added to the organic solution dropwise, and the mixture was allowed to stir at room temperature for 2 h. Once reaction was completed, the mixture was diluted with water, and the pH was adjusted about 3.0. The reaction mixture was extracted with EtOAc for three times, dried over anhydrous sodium sulfate, filtered and evaporated under reduced pressure to obtain compound **6** and **6β+δ**.

2-((7-oxocyclohepta-1,3,5-trien-1-yl)oxy)acetic acid (6). Yellowish solid; m.p. 119–120 °C; 51 % yield. **^{1}H NMR** (600 MHz, DMSO-d_6): δ 4.83 (s, 2H, OCH_2), 6.90 (d, J = 9.9 Hz, 1H, Ar), 6.95 (dd, J = 10.8, 8.2, 1H, Ar), 7.05 (d, J = 12.1, 1H, Ar), 7.13 (m, 1H, Ar), 7.32 (m, 1H, Ar). **^{13}C NMR** (151 MHz, DMSO-d_6): δ 65.6, 115.4, 129.1, 133.5, 137.2, 137.4, 163.8, 169.6, 179.7. Anal. calcd for $C_9H_8O_4$: C, 60.00; H, 4.48. Found: C, 60.09; H, 4.52. Characterization data are in agreement with the previous literature [46].

2-((3-isopropyl-7-oxocyclohepta-1,3,5-trien-1-yl)oxy)acetic acid (6β+δ). β:δ ratio assessed by ^{1}H NMR analysis: 57:43. The reported IUPAC name is referred to as the β isomer. Yellow oil; 80 % yield. **^{1}H NMR** (300 MHz, $CDCl_3$): δ 1.25 (d, J = 7.2 MHz, 6H, CH_3 iPro), 1.30 (d, J = 7.2 MHz, 6H, CH_3 iPro), 2.82–2.90 (m, 1H, CH iPro), 2.91–3.02 (m, 1H, CH iPro), 3.93 (s, 2H, OCH_2), 3.98 (s, 2H, OCH_2), 7.02–7.14 (m, 4H, Ar), 7.19–7.32 (m, 2H, Ar), 7.39–7.46 (m, 1H, Ar). **^{13}C NMR** (75 MHz, $CDCl_3$): δ 22.0, 22.3, 38.4, 38.8, 55.4, 113.5, 115.6, 125.7, 125.7, 129.7, 129.7, 133.0, 133.2, 133.5, 133.5, 138.7, 138.7, 156.4, 160.1, 174.7, 174.7. Anal. calcd for $C_{12}H_{14}O_4$: C, 68.85; H, 6.35. Found: C, 68.80; H, 6.31.

4.1.5. General procedure for the synthesis of compounds 15 and 15δ

p-Nitrobenzoic acid (1.2 equivalents) was added to a stirring mixture of *N,N′*-dicyclohexylcarbodiimide (DCC) (1.5 equivalents) and dimethylaminopyridine (DMAP) (0.2 equivalents) in dry DCM (0.2 M) at room temperature under N_2. After the formation of the intermediate (ca. h), **TRP** or β-**TJP** (1.0 equivalent) was added, and the mixture was stirred for additional 24 h. Then, the reaction mixture was diluted with DCM and filtrated under vacuum to remove *N,N′*-dicyclohexylurea (DCU). The filtrate was then evaporated to give the crude product. The compound was purified through flash column chromatography, employing silica gel and the suitable eluent (mixtures of *n*-hexane/ethyl acetate)

7-Oxocyclohepta-1,3,5-trien-1-yl-4-nitrobenzoate (15). Off-white powder; 80 % yield, m.p. 175–177 °C **^{1}H NMR** (500 MHz, DMSO-d_6): 7.29–7.7.46 (m, 5H, Ar), 8.31 (d, J = 8.3 Hz, 2H, Ar), 8.40 (d, J = 8.8 Hz, 2H, Ar). Melting point data agree with the previous literature [47].

5-isopropyl-7-oxocyclohepta-1,3,5-trien-1-yl 4-nitrobenzoate (15δ). Orange oil; 60 % yield. **^{1}H NMR** (600 MHz, $CDCl_3$): 1.27 (d, J = 6.0 Hz, 6H, CH_3 iPro), 2.81–2.86 (m, 1H, CH iPro), 7.03 (d, J = 12 Hz, 1H, Ar), 7.13 (t, J = 9.0, 6.0 Hz, 1H, Ar), 7.22 (d, J = 12 Hz, 1H, Ar), 7.26 (d, J = 6.0 Hz, 1H, Ar), 8.32–8.36 (m, 4H, Ar). **^{13}C NMR** (151 MHz, $CDCl_3$): δ 23.0, 38.5, 123.7, 131.7, 134.6, 151.0, 162.4. Anal. calcd for $C_{17}H_{15}NO_5$: C, 65.17; H, 4.83; N, 4.47. Found: C, 65.22; H, 4.85; N, 4.50.

4.1.6. General procedure for the synthesis of compounds 16 and 16β+δ

TRP or β-**TJP** (1.0 equivalent) was added to a mixture of triethylamine (TEA) (2.0 equivalents) and DMAP (0.1 equivalents) in DCM (0.25 M) at 0 °C. Then, 1-adamantanecarbonyl chloride was added to the mixture and the yellowish reaction mixture was allowed to stir at room temperature for 48 h. Then, the reaction mixture was poured into water and extracted with DCM three times. The combined organic layers were dried over sodium sulfate anhydrous, filtered, and evaporated *in vacuo* to obtain the crude product. The compound was purified through flash column chromatography, employing silica gel and the suitable eluent (mixtures of DCM/MeOH).

7-oxocyclohepta-1,3,5-trien-1-yl adamantane-1-carboxylate (16). Yellow solid; m.p.: 118–120 °C; 65 % yield. **^{1}H NMR** (300 MHz, $CDCl_3$): δ 1.76 (t, J = 2.7 Hz, 6H, adamantane), 2.08 (d, J = 6.6 Hz, 9H, adamantane), 7.14–7.18 (m, 5H, Ar). **^{13}C NMR** (75 MHz, $CDCl_3$): δ 27.9, 36.4, 38.8, 41.2, 133.0, 133.9, 175.0. Anal. calcd for $C_{18}H_{20}O_3$: C, 76.03; H, 7.09. Found: C, 76.10; H, 7.03.

3-isopropyl-7-oxocyclohepta-1,3,5-trien-1-yl adamantane-1-carboxylate (16β+δ). β:δ ratio assessed by ^{1}H NMR analysis: 85:15. The reported IUPAC name is referred to as the β isomer. Yellow solid; m.p.: 46–48 °C; 41 % yield. **^{1}H NMR** (300 MHz, $CDCl_3$/Acetone mixture): δ 1.40 (d, J = 6.9 Hz, 6H, 2 x CH_3 iPro), 1.44 (d, J = 6.9 Hz, 6H, 2 x CH_3 iPro), 1.93 (s, 12H, adamantane), 2.25 (d, J = 8.4 Hz, 18H, adamantane), 2.91–3.08 (m, 2H, 2 x CH iPro), 7.10–7.11 (m, 2H, Ar), 7.20–7.27 (m, 4H, Ar), 7.43–7.52 (m, 1H, Ar). **^{13}C NMR** (75 MHz, $CDCl_3$): δ 22.9, 23.4 27.8, 28.0, 36.4, 36.5, 38.8, 41.1, 122.3, 132.0, 133.1, 133.5, 155.2, 175.1. Anal. calcd for $C_{21}H_{26}O_3$: C, 77.27; H, 8.03. Found: C, 77.20; H, 8.06.

4.1.7. General procedure for the synthesis of compounds 17, 17β and 17δ

Toluene 4-sulfonyl chloride (1.2 equivalents) in DCM (1.0 M) was added dropwise to a DCM (5.5 M solution of **TRP** or β-**TJP** (1.0 equivalent) and TEA (1.3 equivalents) at 0 °C. Then, the reaction mixture was allowed to stir at room temperature for 5 days. Then, the reaction mixture was poured into water and extracted with DCM three times. The combined organic layers were dried over sodium sulfate anhydrous, filtered, and evaporated *in vacuo* to obtain the crude product. The compound was purified through flash column chromatography, employing silica gel and the suitable eluent (mixtures of *n*-hexane/ethyl acetate).

(7-Oxocyclohepta-1,3,5-trien-1-yl)-4-methylbenzenesulfonate (17) Off-white powder, m.p. 157–159 °C, 88 % yield. **^{1}H NMR** (500 MHz, DMSO-d_6): 2.41 (s, 3H, $ArCH_3$), 7.08–7.11 (m, 2H, Ar), 7.24 (dd, J = 10.8, 8.3 Hz, 1H, Ar), 7.36–7.41 (m, 2H, Ar), 7.46 (d, 1H, J = 8.3 Hz, 2H, Ar), 7.81 (d, 1H, J = 8.3 Hz, 2H, Ar). Characterization data are in agreement with the previous literature [48].

3-isopropyl-7-oxocyclohepta-1,3,5-trien-1-yl 4-methylbenzenesulfonate (17β). White solid, 48 % yield. **^{1}H NMR** (600 MHz, $CDCl_3$): δ 1.23 (d, J = 6.0 Hz, 6H, CH_3 iPro), 2.43 (s, 3H, $ArCH_3$), 2.77–2.82 (m, 1H, CH iPro), 6.91–6.93 (m, 1H, Ar), 7.01–7.03 (m, 1H, Ar), 7.13 (dd, J = 15.0, 6.0 Hz, 1H, Ar), 7.34 (d, J = 6.0 Hz, 2H, Ar), 7.38 (d, J = 6.0 Hz, 1H, Ar), 7.91 (d, J = 12.0 Hz, 2H, Ar). **^{13}C NMR** (151 MHz, $CDCl_3$): δ 21.8, 22.8, 38.2, 128.7, 129.7, 130.4, 131.8, 133.6, 137.0, 139.0, 145.5, 152.5, 154.6, 179.0. Anal. calcd for $C_{17}H_{18}O_4S$: C, 64.13; H, 5.70. Found: C, 64.05; H, 5.75. Characterization data are in agreement with the previous literature [28].

5-isopropyl-7-oxocyclohepta-1,3,5-trien-1-yl 4-methylbenzenesulfonate (17δ). White solid, 58 % yield. **^{1}H NMR** (600 MHz, $CDCl_3$): δ 1.20 (d, J = 6.0 Hz, 6H, CH_3 iPro), 2.44 (s, 3H, $ArCH_3$), 2.72–2.76 (m, 1H, CH iPro), 6.87–6.90 (m, 1H, Ar), 6.87–6.99 (m, 1H, Ar), 7.06–7.07 (m, 1H, Ar), 7.35 (d, J = 6.0 Hz, 3H, Ar), 7.93 (d, J = 6.0 Hz, 2H, Ar). **^{13}C NMR** (151 MHz, $CDCl_3$): δ 21.8, 22.8, 34.5, 128.7, 129.3, 129.6, 129.7, 133.7, 136.6, 138.0, 145.5, 154.8, 157.4, 179.3. Anal. calcd for $C_{17}H_{18}O_4S$: C, 64.13; H, 5.70. Found: C, 64.18; H, 5.72. Characterization data are in agreement with the previous literature [28].

4.2. NMR analysis of regioisomers 10β+δ, 8β+δ, 11β, and 11δ

The solvents used for NMR analysis were purchased from EurIsotop (Saint-Aubin, France). Samples were dissolved in $CDCl_3$ and tetramethylsilane (TMS) was used as an internal reference. Full ^{1}H and ^{13}C assignments were made based on one- and two-dimensional NMR spectra (^{1}H, ^{13}C, COSY, NOESY, HSQC, and HMBC). All spectra were recorded at 25 °C on a Bruker Avance AV600 (Bruker Corporation, Billerica, Massachusetts, US) equipped with a 5 mm diameter BBO probe with a z-gradient accessory. NOESY spectra were obtained with a mixing time of

500 ms. The spectra were acquired using standard Bruker pulse sequences and the data was processed using ACD Spectrus software. Fully assigned NMR spectra with experimental parameters can be found in the Supplementary Material file.

4.3. X-ray crystallography

4.3.1. Crystallization and X-ray data collection

Crystals of the hCA II isoform were obtained using the hanging drop vapor diffusion method in a 24-well VDX plate. 1 μL of 10 mg/mL of hCA II in Tris–HCl 50 mM (pH 8.0) was mixed with 1 μL of a solution of 1.5 M sodium citrate, 20 mM Tris-HCl (pH 8.0) and equilibrated against 500 μL of the same solution at 296 K. Crystal growth was observed after five days. The protein complex with β-**TJP** was prepared by soaking the crystals in the mother liquor solution containing the inhibitor at a concentration of 10 mM for 3 h. Then, all crystals were flash-frozen at 100 K using a solution obtained by adding 15 % (*v/v*) PEG 400 to the mother liquor solution as a cryoprotectant. X-ray diffraction data were collected using synchrotron radiation at the ID30B beamline at ESRF (Grenoble, France) with a wavelength of 0.87313 Å and a DECTRIS Eiger2 X 9 M detector.

4.3.2. Structure determination

The crystal structures of hCA II (PDB ID: 3HS4) without solvent molecules and other heteroatoms were used to obtain the initial phases of the structures using Refmac5 [49] from the CCP4 package [50]. Coordinates of the inhibitor were obtained using the program JLigand [51] and introduced in the model. 5 % of the unique reflections were selected randomly and excluded from the refinement data set for R_{free} calculations. The initial |Fo–Fc| difference electron density maps unambiguously showed the inhibitor molecules. The inhibitor was introduced in the model with 1.0 occupancy. Refinements proceeded using standard protocols of positional, and isotropic atomic displacement parameters alternating with the manual building of the models using COOT [52]. Inhibitor-enzyme interactions were analyzed using the PLIP web tool [53]. Atomic coordinates were deposited in the PDB (PDB ID: 9H0W) and reported in Table 2. Graphical representations were generated with UCSF Chimera [54].

Table 2
Summary of data collection and atomic model refinement statistics for hCA II.

Data collection statistics	
	hCA II-β-TJP
PDB ID	9H0W
Wavelength (Å)	0.87313
Space Group	P 1 21 1
Unit cell (a, b, c, α, β, γ) (Å,°)	42.23, 41.05, 71.92, 90, 104.26, 90
Limiting resolution (Å)	41.05–1.44 (1.46–1.44)
Unique reflections	43458 (2148)
Rmerge	0.094 (1.250)
Rmeas	0.102 (1.355)
Redundancy	6.7 (6.8)
Completeness overall (%)	99.9 (100.0)
<I/σ(I)>	11.8 (1.5)
CC (1/2)	0.999 (0.522)
Refinement statistics	
Resolution range (Å)	41.05–1.44
Rfactor	0.1656
Rfree	0.1958
r.m.s.d. bonds (Å)	0.0105
r.m.s.d. angles (°)	1.9004
Ramachandran statistics (%)	
Most favored	97.3
additionally allowed	2.7
Outlier regions	0.0
Average B factor (Å^2)	
All atoms	20.83
Inhibitor	23.00
Solvent	29.41

4.4. Carbonic anhydrases inhibition assays

An Applied Photophysics stopped-flow instrument was used to evaluate the ability of the test compounds to inhibit the CA-catalyzed CO_2 hydration [33]. 0.2 mM Phenol red was chosen as an indicator (absorbance maximum = 557 nm), with 20 mM HEPES (pH 7.4) as a buffer, and 20 mM Na_2SO_4 (to maintain constant the ionic strength), following the initial rates of the CA-catalyzed CO_2 hydration reaction for a period of 10–100 s. The CO_2 concentrations ranged from 1.7 to 17 mM for the determination of the kinetic parameters and inhibition constants. Enzyme concentrations spanned from 5 to 12 nM. Stock solutions of the inhibitor (0.1 mM) were prepared in distilled–deionized water and dilutions up to 0.01 nM were prepared with the assay buffer. Inhibitor and enzyme solutions were preincubated for 15 min at r.t. for the formation of the E–I complex. The inhibition constants were obtained by non-linear least-squares methods using PRISM 3 and the Cheng-Prusoff equation and represent the mean from at least three different determinations. Apart from hCAs I and II purchased from Merck, all the other CAs are recombinant and obtained *in-house*. [55–57].

4.5. Molecular modeling

4.5.1. Library preparation

The library of the compound was prepared by means of the LigPrep tool. Hydrogens were added, salts were removed, and ionization states were calculated using Epik at pH 7.4 ± 0.2 and then were submitted to MacroModel energy minimization, using OPLS_2005 as force field [58, 59].

4.5.2. Target preparation

The X-ray crystallographic structures of hCAs I, II, VII, IX, and XII isoforms were retrieved from the PDB IDs: 2NMX, 3K34, 3ML5, 5FL4, and 1JD0, respectively. For the hCA VA isoform, the model prepared according to our previously published work was used [60]. The receptor structures were optimized by means of the Protein Preparation Wizard tool [61], using OLPS_2005 as the force field. Residual crystallographic buffer components and water molecules were removed, hydrogen atoms were added, missing side chains were built using the Prime module, and side chains protonation states at pH 7.4 were assigned.

4.5.3. Molecular docking and eMBrAcE studies

In order to evaluate the reliability of our molecular recognition approach, redocking calculations by using the Glide Standard Protocol (SP) algorithm were performed. As reported in Table 3, Root Mean Square Deviation (RMSD) values, calculated between the best docking pose and the ligand co-crystallized into the catalytic binding site, demonstrate a reproduction of the experimentally determined binding modes for all examined models.

Molecular docking was carried out with Glide v. 8.9 software, by using the Standard Precision (SP) algorithm, and 25 poses per ligand were generated. [62,63]. Starting from the best docking pose of each compound post-docking energy minimization was performed by using the eMBrAcE tool [64] and the binding energies (E) of the receptor-ligand complexes were calculated [65].

Table 3
PDB IDs and RMSD values calculated between the best docking pose and the ligand co-crystallized.

hCA isoform	PDB IDs	RMSD values (Å)
I	2NMX	1.01
II	3K34	1.13
VII	3ML5	0.33
IX	5FL4	0.27
XII	1JD0	0.63

4.6. Chemical stability

5.0 mg of **17β** were dissolved in 0.5 mL of DMSO-d_6/D_2O 1/1 *v/v* and ^1H NMR spectra were recorded at t_0, 4, 6, 24, 48, 72, and 120 h to assess chemical stability of the sulfonate ester.

4.7. Antiproliferative assays

4.7.1. MM cell lines

MM cell lines NCI–H929, U266, MM1S, and JJN3 were purchased from DSMZ, with certified authentication performed by short tandem repeat DNA typing. NCI–H929 cells resistant to BZB (namely NCI–H929 BZB) and CFZ (namely NCI–H929 CFZ) were obtained following progressive exposure to increasing concentrations of proteasome inhibitors and kept at the final concentration of 20 nM of the two drugs. AMO and AMO BZB cells were kindly provided by Dr. C. Driessen (University of Tubingen, Germany). KMS26, KMS26 BZB were kindly provided by Prof. Antonino Neri (University of Milan).

All these cell lines were immediately frozen and used from the original stock within 6 months. Cells were cultured in RPMI-1640 medium enriched with 10 % heat-inactivated fetal bovine serum (FBS) (Gibco®, Life Technologies, Carlsbad, CA), 100 μg/mL streptomycin (P/S) (Gibco®, Life Technologies, Carlsbad, CA), and 100 U/mL of penicillin. MM cells were incubated at 37 °C in a 5 % CO_2 atmosphere; for hypoxic conditions, cells were incubated in a dedicated Eppendorf Galaxy 48R incubator in 1 % O_2.

PBMCs were isolated using Ficoll-Hypaque density gradient sedimentation (Lonza Group, Basel, Switzerland), following the approval of the Institutional Review Board n. 266/2021 (University of Catanzaro, Italy).

4.7.2. Western blotting

Cell lysis was performed in NP40 Cell Lysis Buffer supplemented with Halt Protease Inhibitor Single-Use Cocktail (Thermo Fisher Scientific, Waltham, MA, USA). Protein samples (30 μg) were subjected to 10 % SDS-PAGE, and the gels were dry-transferred onto nitrocellulose membranes using the Trans-Blot Turbo Transfer System (Bio-Rad Laboratories, Hercules, CA, USA), followed by incubation with following Abs purchased from Cell Signaling Technology: CA IX (#5649S), CA XII (#5864S), GAPDH (#5174). Densitometry was performed using the ImageJ software.

4.7.3. Cell viability assay

Cell viability was evaluated by Cell Titer Glo (CTG) assay kit (Promega, Madison, WI, USA), according to manufacturer's instructions. Briefly, MM cells were seeded in 24-well plates and, after 48 h of treatment with tropolonoids, collected and plated in 96 well white plates. Treated cells were incubated in both normoxic and hypoxic conditions. Luminescence was recorded using the GloMax Multi Detection System (Promega, Madison, WI, USA). IC_{50} values were evaluated using GraphPad Prism software.

4.7.4. Apoptosis assay

Apoptosis was evaluated by Annexin-V/7-Aminoactinomycin D (7-AAD) staining and flow cytometric analysis using the PE Annexin-V Apoptosis Detection Kit I (Thermo Fisher Scientific, Waltham, MA, USA). After treatment with 16β compound, MM cells were collected in a 5 mL polystyrene tube, washed with PBS 1X, and exposed to Annexin V-PE and 7-AAD probes for 15 min at room temperature. After incubation, the samples were analyzed using a FACS Fortessa X-20 instrument (BD Biosciences, San Jose, CA, USA), and the data were analyzed using FlowJo software version 10. The histogram bars indicate the percentage of early and late apoptotic cells.

CRediT authorship contribution statement

Francesco Melfi: Formal analysis. **Ilaria D'Agostino:** Formal analysis. **Simone Carradori:** Conceptualization. **Fabrizio Carta:** Writing – original draft. **Andrea Angeli:** Formal analysis. **Giosuè Costa:** Methodology. **Gioele Renzi:** Methodology. **Ana Čikoš:** Formal analysis. **Daniela Vullo:** Formal analysis. **Josip Rešetar:** Formal analysis. **Marta Ferraroni:** Formal analysis. **Chiara Baroni:** Formal analysis. **Francesca Mancuso:** Formal analysis. **Rosaria Gitto:** Writing – review & editing. **Francesca Alessandra Ambrosio:** Formal analysis. **Emanuela Marchese:** Investigation. **Roberta Torcasio:** Investigation. **Nicola Amodio:** Resources, Methodology, Investigation, Formal analysis. **Clemente Capasso:** Writing – original draft, Formal analysis, Data curation. **Stefano Alcaro:** Writing – review & editing, Supervision, Data curation. **Claudiu T. Supuran:** Writing – review & editing, Supervision, Funding acquisition, Conceptualization.

Declaration of competing interest

The authors declare that they have no known competing financial interests or personal relationships that could have appeared to influence the work reported in this paper.

The authors declare no competing interests.

Data availability

Additional data could be made available on request to the corresponding authors.

Funding sources

This work was supported by a grant from the Italian Ministry of University and Research for financial support under the FISR program, project FISR_04819 BacCAD to C.T.S., C.C., and S.C. N.A. was supported by an AIRC IG24449 grant.

Declaration of competing interest

The authors declare the following financial interests/personal relationships which may be considered as potential competing interests: Simone Carradori reports financial support was provided by Italian Ministry of University and Research. This work was supported by a grant from the Italian Ministry of University and Research for financial support under the FISR program, project FISR_04819 BacCAD to C.T.S., C. C., and S.C. N.A. was supported by an AIRC IG24449 grant If there are other authors, they declare that they have no known competing financial interests or personal relationships that could have appeared to influence the work reported in this paper.

Acknowledgements

This research was partially supported by the Italian Ministry for University and Research (MIUR) grant number FISR2019_04819 BacCAD to S.C., C.C. and C.T.S. This article is based upon work from COST Action EURESTOP, CA21145, supported by COST (European Cooperation in Science and Technology) to S.C., A.C., and I.D.A. N.A. was supported by an AIRC IG24449 grant.

Appendix A. Supplementary data

Supplementary data to this article can be found online at https://doi.org/10.1016/j.ejmech.2025.117552.

Data availability

Data will be made available on request.

References

[1] M. Ebisawa, K. Ohta, E. Kawachi, H. Fukasawa, Y. Hashimoto, H. Kagechika, Novel retinoidal tropolone derivatives. Bioisosteric relationship of tropolone ring with benzoic acid moiety in retinoid structure, Chem. Pharm. Bull. (Tokyo) 49 (2001) 501–503, https://doi.org/10.1248/cpb.49.501.

[2] F. Pietra, Seven-membered conjugated carbo- and heterocyclic compounds and their homoconjugated analogs and metal complexes. Synthesis, biosynthesis, structure, and reactivity, Chem. Rev. 73 (1973) 293–364, https://doi.org/10.1021/cr60284a002.

[3] B.L. Dick, A. Patel, J.A. McCammon, S.M. Cohen, Effect of donor atom identity on metal-binding pharmacophore coordination, J. Biol. Inorg. Chem. 22 (2017) 605–613, https://doi.org/10.1007/s00775-017-1454-3.

[4] K. Azegami, K. Nishiyama, Y. Watanabe, T. Suzuki, M. Yoshida, K. Nose, S. Toda, Tropolone as a Root growth-inhibitor produced by a plant pathogenic Pseudomonas sp. causing seedling blight of rice, Jpn. J. Phytopathol. 51 (1985) 315–317, https://doi.org/10.3186/jjphytopath.51.315.

[5] P.L. Pauson, Tropones and tropolones, Chem. Rev. 55 (1955) 9–136, https://doi.org/10.1021/cr50001a002.

[6] N. Liu, W. Song, C.M. Schienebeck, M. Zhang, W. Tang, Synthesis of naturally occurring tropones and tropolones, Tetrahedron 70 (2014) 9281–9305, https://doi.org/10.1016/j.tet.2014.07.065.

[7] R.P. Murelli, A.J. Berkowitz, D.W. Zuschlag, Carbocycloaddition strategies for troponoid synthesis, Tetrahedron 130 (2023) 133175, https://doi.org/10.1016/j.tet.2022.133175.

[8] R. Bentley, A fresh look at natural tropolonoids, Nat. Prod. Rep. 25 (2008) 118–138, https://doi.org/10.1039/b711474e.

[9] J. Zhao, Plant troponoids: chemistry, biological activity, and biosynthesis, Curr. Med. Chem. 14 (2007) 2597–2621, https://doi.org/10.2174/092986707782023253.

[10] W.-K. Wang, S.-T. Lin, W.-W. Chang, L.-W. Liu, T.Y.-T. Li, C.-Y. Kuo, J.-L. Hsieh, C.-H. Lee, Hinokitiol induces autophagy in murine breast and colorectal cancer cells, Environ. Toxicol. 31 (2016) 77–84, https://doi.org/10.1002/tox.22023.

[11] Y. Inoue, R. Suzuki, I. Murata, H. Nomura, Y. Isshiki, I. Kanamoto, Evaluation of antibacterial activity expression of the hinokitiol/cyclodextrin complex against bacteria, ACS Omega 5 (2020) 27180–27187, https://doi.org/10.1021/acsomega.0c03222.

[12] T.J. Trust, Antibacterial activity of tropolone, Antimicrob. Agents Chemother. 7 (1975) 500–506, https://doi.org/10.1128/AAC.7.5.500.

[13] S.L. Haney, M.L. Varney, H.R. Safranek, Y.S. Chhonker, N. G-Dayanandan, G. Talmon, D.J. Murry, A.J. Wiemer, D.L. Wright, S.A. Holstein, Tropolone-induced effects on the unfolded protein response pathway and apoptosis in multiple myeloma cells are dependent on iron, Leuk. Res. 77 (2019) 17–27, https://doi.org/10.1016/j.leukres.2018.12.007.

[14] J.L. Fullagar, A.L. Garner, A.K. Struss, J.A. Day, D.P. Martin, J. Yu, X. Cai, K. D. Janda, S.M. Cohen, Antagonism of a zinc metalloprotease using a unique metal-chelating scaffold: tropolones as inhibitors of P. aeruginosa elastase, Chem. Commun. Camb. Engl. 49 (2013) 3197–3199, https://doi.org/10.1039/c3cc41191e.

[15] K.M. Varier, T. Sumathi, Hinokitiol offers neuroprotection against 6-OHDA-induced toxicity in SH-SY5Y neuroblastoma cells by downregulating mRNA expression of MAO/α-Synuclein/LRRK2/PARK7/PINK1/PTEN genes, Neurotox. Res. 35 (2019) 945–954, https://doi.org/10.1007/s12640-018-9988-x.

[16] H. Domon, T. Hiyoshi, T. Maekawa, D. Yonezawa, H. Tamura, S. Kawabata, K. Yanagihara, O. Kimura, E. Kunitomo, Y. Terao, Antibacterial activity of hinokitiol against both antibiotic-resistant and -susceptible pathogenic bacteria that predominate in the oral cavity and upper airways, Microbiol. Immunol. 63 (2019) 213–222, https://doi.org/10.1111/1348-0421.12688.

[17] G. Zhang, J. He, X. Ye, J. Zhu, X. Hu, M. Shen, Y. Ma, Z. Mao, H. Song, F. Chen, β-Thujaplicin induces autophagic cell death, apoptosis, and cell cycle arrest through ROS-mediated Akt and p38/ERK MAPK signaling in human hepatocellular carcinoma, Cell Death Dis. 10 (2019) 255, https://doi.org/10.1038/s41419-019-1492-6.

[18] Y. Naito, Y. Yoshikawa, M. Shintani, S. Kamoshida, N. Kajiwara, H. Yasui, Anti-hyperglycemic effect of long-term bis(hinokitiolato)zinc complex ([Zn(hkt)2]) ingestion on insulin resistance and pancreatic islet cells protection in type 2 diabetic KK-Ay Mice, Biol. Pharm. Bull. 40 (2017) 318–326, https://doi.org/10.1248/bpb.b16-00797.

[19] E.L. Muetterties, H. Roesky, C.M. Wright, Chelate chemistry. V. Metal chelates based on tropolone and its derivatives, J. Am. Chem. Soc. 88 (1966) 4856–4861, https://doi.org/10.1021/ja00973a019.

[20] B.X. Hoang, B. Han, A possible application of hinokitiol as a natural zinc ionophore and anti-infective agent for the prevention and treatment of COVID-19 and viral infections, Med. Hypotheses 145 (2020) 110333, https://doi.org/10.1016/j.mehy.2020.110333.

[21] J. Gerke, A.M. Köhler, J.-P. Wennrich, V. Große, L. Shao, A.K. Heinrich, H.B. Bode, W. Chen, F. Surup, G.H. Braus, Biosynthesis of antibacterial iron-chelating tropolones in Aspergillus nidulans as response to glycopeptide-producing Streptomycetes, Front. Fungal Biol 2 (2021) 777474, https://doi.org/10.3389/ffunb.2021.777474.

[22] X. Lai, H.J. Wichers, M. Soler-Lopez, B.W. Dijkstra, Structure of human tyrosinase related protein 1 reveals a binuclear zinc active site important for Melanogenesis, Angew Chem. Int. Ed. Engl. 56 (2017) 9812–9815, https://doi.org/10.1002/anie.201704616.

[23] P.J. Gawne, F. Man, P.J. Blower, R. T M de Rosales, Direct cell radiolabeling for in vivo cell Tracking with PET and SPECT Imaging, Chem. Rev. 122 (2022) 10266–10318, https://doi.org/10.1021/acs.chemrev.1c00767.

[24] D.P. Martin, Z.S. Hann, S.M. Cohen, Metalloprotein-inhibitor binding: human carbonic anhydrase II as a model for probing metal-ligand interactions in a metalloprotein active site, Inorg. Chem. 52 (2013) 12207–12215, https://doi.org/10.1021/ic400295f.

[25] G. Costa, M.C. Gidaro, D. Vullo, C.T. Supuran, S. Alcaro, Active components of essential oils as anti-obesity potential drugs investigated by in silico techniques, J. Agric. Food Chem. 64 (2016) 5295–5300, https://doi.org/10.1021/acs.jafc.6b02004.

[26] I. Tamburlin-Thumin, M.P. Crozet, J.C. Barrière, M. Barreau, J.F. Riou, F. Lavelle, Synthesis and biological evaluation of O-alkylated tropolones and related alpha-ketohydroxy derivatives as ribonucleotide reductase inhibitors, Eur. J. Med. Chem. 36 (2001) 561–568, https://doi.org/10.1016/s0223-5234(01)01249-1.

[27] M. Cavazza, F. Pietra, Tautomeric selectivity towards colchicinoids in the tosylation of colchiceine on a heterogeneous, easily removable catalyst, Org. Biomol. Chem. 1 (2003) 3002–3003, https://doi.org/10.1039/b307650b.

[28] M. Elagawany, L. Hegazy, F. Cao, M.J. Donlin, N. Rath, J. Tavis, B. Elgendy, Identification of 4-isopropyl-thiotropolone as a novel anti-microbial: regioselective synthesis, NMR characterization, and biological evaluation, RSC Adv. 8 (2018) 29967–29975, https://doi.org/10.1039/c8ra06297h.

[29] M. Fantacuzzi, I. D'Agostino, S. Carradori, F. Liguori, F. Carta, M. Agamennone, A. Angeli, F. Sannio, J.-D. Docquier, C. Capasso, C.T. Supuran, Benzenesulfonamide derivatives as Vibrio cholerae carbonic anhydrases inhibitors: a computational-aided insight in the structural rigidity-activity relationships, J. Enzym. Inhib. Med. Chem. 38 (2023) 2201402, https://doi.org/10.1080/14756366.2023.2201402.

[30] G. Benito, I. D'Agostino, S. Carradori, M. Fantacuzzi, M. Agamennone, V. Puca, R. Grande, C. Capasso, F. Carta, C.T. Supuran, Erlotinib-containing benzenesulfonamides as anti-Helicobacter pylori agents through carbonic anhydrase inhibition, Future Med. Chem. 15 (2023) 1865–1883, https://doi.org/10.4155/fmc-2023-0208.

[31] V.L. Hideko Tatakihara, A.D. Malvezi, R.S. Pereira, B.F.C. Lucchetti, L.F. Dos Santos, R. Cecchini, L.M. Yamauchi, S.F. Yamada-Ogatta, K.M. Miranda, W. A. Verri, M.C. Martins-Pinge, P. Pinge-Filho, The Therapeutic potential of Angeli's salt in mitigating Acute Trypanosoma cruzi infection in mice, Pathog. Basel Switz. 12 (2023) 1063, https://doi.org/10.3390/pathogens12081063.

[32] A. Angeli, M. Ferraroni, A.A. Da'dara, S. Selleri, M. Pinteala, F. Carta, P.J. Skelly, C.T. Supuran, Structural insights into Schistosoma mansoni carbonic anhydrase (SmCA) inhibition by Selenoureido-substituted benzenesulfonamides, J. Med. Chem. 64 (2021) 10418–10428, https://doi.org/10.1021/acs.jmedchem.1c00840.

[33] R.G. Khalifah, The carbon dioxide hydration activity of carbonic anhydrase. I. Stop-flow kinetic studies on the native human isoenzymes B and C, J. Biol. Chem. 246 (1971) 2561–2573.

[34] H. Aslan, G. Renzi, A. Angeli, I. D'Agostino, R. Ronca, M. Massardi, C. Tavani, S. Carradori, M. Ferraroni, P. Governa, F. Manetti, F. Carta, C. Supuran, Benzenesulfonamide Decorated Dihydropyrimidin(thi)ones: carbonic anhydrase profiling and antiproliferative activity, RSC Med. Chem. 15 (2024) 1929–1941, https://doi.org/10.1039/D4MD00101J.

[35] J.T. Kilbile, S.B. Sapkal, G. Renzi, I. D'Agostino, L. Cutarella, M. Mori, B. De Filippis, I. Islam, M.L. Massardi, E. Somenza, R. Ronca, Y. Tamboli, F. Carta, C. T. Supuran, Novel 2,4-Dichloro-5-sulfamoylbenzoic acid Oxime esters: first studies as potential human carbonic anhydrase inhibitors, ACS Med. Chem. Lett. 15 (2024) 972–978, https://doi.org/10.1021/acsmedchemlett.4c00206.

[36] M. Agamennone, M. Fantacuzzi, S. Carradori, A. Petzer, J.P. Petzer, A. Angeli, C. T. Supuran, G. Luisi, Coumarin-based dual inhibitors of human carbonic anhydrases and Monoamine Oxidases featuring Amino acyl and (Pseudo)-Dipeptidyl Appendages: in vitro and computational studies, Mol. Basel Switz. 27 (2022) 7884, https://doi.org/10.3390/molecules27227884.

[37] A. Nocentini, A. Angeli, F. Carta, J.-Y. Winum, R. Zalubovskis, S. Carradori, C. Capasso, W.A. Donald, C.T. Supuran, Reconsidering anion inhibitors in the general context of drug design studies of modulators of activity of the classical enzyme carbonic anhydrase, J. Enzym. Inhib. Med. Chem. 36 (2021) 561–580, https://doi.org/10.1080/14756366.2021.1882453.

[38] A. Karioti, F. Carta, C.T. Supuran, Phenols and polyphenols as carbonic anhydrase inhibitors, Molecules 21 (2016) 1649, https://doi.org/10.3390/molecules21121649.

[39] R. Paciotti, S. Carradori, A. Angeli, I. D'Agostino, M. Ferraroni, C. Coletti, C. T. Supuran, Unprecedented carbonic anhydrase inhibition mechanism: Targeting histidine 64 side chain through a halogen bond, Arch. Pharm. (Weinheim) 358 (2025) e2400776, https://doi.org/10.1002/ardp.202400776.

[40] E. Taiana, M.E. Gallo Cantafio, V.K. Favasuli, C. Bandini, G. Viglietto, R. Piva, A. Neri, N. Amodio, Genomic instability in multiple myeloma: a "Non-coding RNA" perspective, Cancers 13 (2021) 2127, https://doi.org/10.3390/cancers13092127.

[41] K. D'Ambrosio, A. Di Fiore, V. Alterio, E. Langella, S.M. Monti, C.T. Supuran, G. De Simone, Multiple binding modes of inhibitors to human carbonic anhydrases: an update on the design of isoform-specific modulators of activity, Chem. Rev. 125 (2025) 150–222, https://doi.org/10.1021/acs.chemrev.4c00278.

[42] G. Navarro, M. Gómez-Autet, P. Morales, J.B. Rebassa, C. Llinas Del Torrent, N. Jagerovic, L. Pardo, R. Franco, Homodimerization of CB2 cannabinoid receptor triggered by a bivalent ligand enhances cellular signaling, Pharmacol. Res. 208 (2024) 107363, https://doi.org/10.1016/j.phrs.2024.107363.

[43] A. Pryde, J. Zsindely, H. Schmid, Thermische Umlagerung von Propargyloxy-cycloheptatrien-Derivaten, Helv. Chim. Acta 57 (1974) 1598–1613, https://doi.org/10.1002/hlca.19740570614.

[44] H. Takeshita, A. Mori, H. Suizu, Novel Base-Promoted Rearrangement of 2-(4-Cyano-, 2-Nitro-, and 4-Nitrobenzyloxy)tropones and 2-(2-Oxo-2-phenethyloxy)tropone to 2-[(4-Cyano-, 2-Nitro-, and 4-Nitrophenyl)hydroxymethyl]tropones and 2-(1-Hydroxy-2-oxo-2-phenethyl)tropone, Bull. Chem. Soc. Jpn. 60 (1987) 1429–1432, https://doi.org/10.1246/bcsj.60.1429.
[45] H. Takeshita, A. Mori, H. Suizu, An anion-promoted rearrangement of 2-(o- and p-nitrobenzyloxy)tropones to α-hydroxylated 2-(o- and p-nitrobenzyl)tropones. A ready introduction of aralkyl group into the troponoid nucleuS, Chem. Lett. 15 (1986) 593–596, https://doi.org/10.1246/cl.1986.593.
[46] J.R. Scheffer, L. Wang, Enantioselective photoelectrocyclization of a tropolone derivative in the crystalline state, J. Phys. Org. Chem. 13 (2000) 531–538, https://doi.org/10.1002/1099-1395(200009)13:9<531::AID-POC293>3.0.CO, 2-5.
[47] R.J. Cornell, L.G. Donaruma, 2-Methacryloxytropones. Intermediates for the synthesis of biologically active polymers, J. Med. Chem. 8 (1965) 388–390, https://doi.org/10.1021/jm00327a025.
[48] K.B. Daniel, J.L. Major Jourden, K.E. Negoescu, S.M. Cohen, Activation of sulfonate ester based matrix metalloproteinase proinhibitors by hydrogen peroxide, JBIC, J. Biol. Inorg. Chem. 16 (2011) 313–323, https://doi.org/10.1007/s00775-010-0727-x.
[49] G.N. Murshudov, A.A. Vagin, E.J. Dodson, Refinement of macromolecular structures by the maximum-likelihood method, Acta Crystallogr. D Biol. Crystallogr. 53 (1997) 240–255, https://doi.org/10.1107/S0907444996012255.
[50] M.D. Winn, C.C. Ballard, K.D. Cowtan, E.J. Dodson, P. Emsley, P.R. Evans, R. M. Keegan, E.B. Krissinel, A.G.W. Leslie, A. McCoy, S.J. McNicholas, G. N. Murshudov, N.S. Pannu, E.A. Potterton, H.R. Powell, R.J. Read, A. Vagin, K. S. Wilson, Overview of the CCP4 suite and current developments, Acta Crystallogr. D Biol. Crystallogr. 67 (2011) 235–242, https://doi.org/10.1107/S0907444910045749.
[51] A.A. Lebedev, P. Young, M.N. Isupov, O.V. Moroz, A.A. Vagin, G.N. Murshudov, JLigand: a graphical tool for the CCP4 template-restraint library, Acta Crystallogr. D Biol. Crystallogr. 68 (2012) 431–440, https://doi.org/10.1107/S090744491200251X.
[52] P. Emsley, B. Lohkamp, W.G. Scott, K. Cowtan, Features and development of coot, Acta Crystallogr. D Biol. Crystallogr. 66 (2010) 486–501, https://doi.org/10.1107/S0907444910007493.
[53] M.F. Adasme, K.L. Linnemann, S.N. Bolz, F. Kaiser, S. Salentin, V.J. Haupt, M. Schroeder, Plip 2021: expanding the scope of the protein-ligand interaction profiler to DNA and RNA, Nucleic Acids Res. 49 (2021) W530–W534, https://doi.org/10.1093/nar/gkab294.
[54] E.F. Pettersen, T.D. Goddard, C.C. Huang, G.S. Couch, D.M. Greenblatt, E.C. Meng, T.E. Ferrin, UCSF Chimera–a visualization system for exploratory research and analysis, J. Comput. Chem. 25 (2004) 1605–1612, https://doi.org/10.1002/jcc.20084.
[55] I. D'Agostino, G.E. Mathew, P. Angelini, R. Venanzoni, G. Angeles Flores, A. Angeli, S. Carradori, B. Marinacci, L. Menghini, M.A. Abdelgawad, M. M. Ghoneim, B. Mathew, C.T. Supuran, Biological investigation of N-methyl thiosemicarbazones as antimicrobial agents and bacterial carbonic anhydrases inhibitors, J. Enzym. Inhib. Med. Chem. 37 (2022) 986–993, https://doi.org/10.1080/14756366.2022.2055009.
[56] I. D'Agostino, A. Bonardi, M. Ferraroni, P. Gratteri, A. Angeli, C.T. Supuran, Exploring the polypharmacological potential of PCI-27483: a selective inhibitor of carbonic anhydrases IX and XII, ACS Med. Chem. Lett. 15 (2024) 2042–2045, https://doi.org/10.1021/acsmedchemlett.4c00443.
[57] B. Marinacci, I. D'Agostino, A. Angeli, S. Carradori, F. Melfi, R. Grande, M. Corsiani, M. Ferraroni, M. Agamennone, A.R. Tondo, S. Zara, V. Puca, B. Pellegrini, C. Vagaggini, E. Dreassi, M.A. Patrauchan, C. Capasso, O. Nicolotti, F. Carta, C.T. Supuran, Inhibition of Pseudomonas aeruginosa carbonic anhydrases, exploring Ciprofloxacin functionalization toward new antibacterial agents: an in-depth multidisciplinary study, J. Med. Chem. 67 (2024) 19077–19102, https://doi.org/10.1021/acs.jmedchem.4c01555.
[58] W.L. Jorgensen, D.S. Maxwell, J. Tirado-Rives, Development and testing of the OPLS all-atom force field on Conformational Energetics and properties of organic liquids, J. Am. Chem. Soc. 118 (1996) 11225–11236, https://doi.org/10.1021/ja9621760.
[59] LigPrep, Schrödinger, LLC, New York, NY, 2024.
[60] G. Costa, F. Carta, F.A. Ambrosio, A. Artese, F. Ortuso, F. Moraca, R. Rocca, I. Romeo, A. Lupia, A. Maruca, D. Bagetta, R. Catalano, D. Vullo, S. Alcaro, C. T. Supuran, A computer-assisted discovery of novel potential anti-obesity compounds as selective carbonic anhydrase VA inhibitors, Eur. J. Med. Chem. 181 (2019) 111565, https://doi.org/10.1016/j.ejmech.2019.111565.
[61] Schrödinger release 2024-4: protein preparation Wizard, Epik, Schrödinger, LLC, New York, NY, 2024; Impact, Schrödinger, LLC, New York, NY; Prime, Schrödinger, LLC, New York, NY, 2024.
[62] R.A. Friesner, J.L. Banks, R.B. Murphy, T.A. Halgren, J.J. Klicic, D.T. Mainz, M. P. Repasky, E.H. Knoll, M. Shelley, J.K. Perry, D.E. Shaw, P. Francis, P.S. Shenkin, Glide: a new approach for rapid, Accurate docking and scoring. 1. Method and assessment of docking accuracy, J. Med. Chem. 47 (2004) 1739–1749, https://doi.org/10.1021/jm0306430.
[63] Schrödinger Release 2024-4: Glide, Schrödinger, LLC, New York, NY, 2024.
[64] Schrödinger Release 2024-4: MacroModel, Schrödinger, LLC, New York, NY, 2024.
[65] F. Mohamadi, N.G.J. Richards, W.C. Guida, R. Liskamp, M. Lipton, C. Caufield, G. Chang, T. Hendrickson, W.C. Still, Macromodel—an integrated software system for modeling organic and bioorganic molecules using molecular mechanics, J. Comput. Chem. 11 (1990) 440–467, https://doi.org/10.1002/jcc.540110405.